1963

A study of the influence of some processing variables on the performance of the fuel electrode of a fuel cell

John Russel Thompson Jr.
Lehigh University

A Study of the Influence of Some Processing Variables on the Performance of the Fuel Electrode of a Fuel Cell

by

John Russell Thompson, Jr.

A Thesis

Presented to the Graduate Faculty

of Lehigh University

in Candidacy for the Degree of

Master of Science

Lehigh University

1963

Certificate of Approval

This Thesis is accepted and approved in partial fulfillment of the requirements for the degree of Master of Science

May 22, 1963
(Date)

George P. Conrad
Professor in Charge

T. F. Kubosh
Head of the Department of
Metallurgical Engineering

ACKNOWLEDGMENTS

The author wishes to express his sincere appreciation to Dr. G. P. Conard, II, Project Director and Professor in Charge, for his technical guidance and encouragement throughout the course of this work. Also to Dr. J. F. Libsch and Dr. H. Suprinick (presently of The State University of New York at Buffalo) for their most helpful ideas and discussions.

This work could not have been undertaken without the help of the Sun Oil Company who provided the financial aid and most of the materials and equipment required. In particular, the author wishes to acknowledge the help offered by Doctors Loveland, Bravo, and Barmby, and Mr. Dimeler.

Special appreciation is extended to Mr. M. M. Sheska and his assistants, Messrs. Horoschock, Mohylsky, and Rice, for their assistance in this endeavor; to Mr. P. P. Podgursky and Mr. J. D. Haselton for their timely assistance; to Mr. G. C. Horak and the Mining Department of Lehigh University for permitting the author to use some of their ore crushing equipment; and last but not least, to the members of the Von Laue Society for their never failing moral support.

TABLE OF CONTENTS

LIST OF FIGURES

LIST OF TABLES

INTRODUCTION

Improved power source and energy conversion systems represent one of the most important long-range problems facing the world. A rapidly increasing population and an increasing per capita usage of energy, coupled with declining fuel reserves, poses this serious problem. This problem is leading us to direct energy conversion systems.

A. COMPARISON OF DIRECT ENERGY SYSTEMS WITH CONVENTIONAL SYSTEMS FOR CONVERTING ENERGY (1-4)

The conversion of the chemical energy of a fuel into electrical energy by conventional means suffers from an unavoidable limitation imposed by thermodynamics. This limitation applies to any process converting heat into work and derives from the nature of heat itself. When heat is converted into another form of energy, it must fall from an absolute temperature T_h to an absolute temperature T_c, and the maximum fraction that can be converted under ideal conditions is $\frac{T_h - T_c}{T_h}$. This is the Carnot efficiency.

Conversion of the chemical energy of a fuel into electrical energy by electrochemical means never involves the conversion of heat into work. The process is essentially isothermal and escapes the Carnot limitations.

The thermodynamic principles are represented by the relationship

$$\Delta G = \Delta H - T\Delta S$$

where ΔG is the free energy change of the system. The maximum electrical work which can be obtained under reversible operation of the cell is equal to ΔG. Thus the efficiency in the ideal case is

$$\eta \text{ id} = \frac{\Delta G}{\Delta H} = 1 - \frac{T\Delta S}{\Delta H}$$

The maximum possible efficiency then depends on the entropy.

Given an electrochemical system, one is more likely to be interested in the efficiency on the basis of

$$\Delta G = -nE^{\circ}F$$

where n is the number of electrons involved in the reaction, F is the Faraday constant, and E° the theoretical voltage. Thus, our ideal efficiency becomes

$$\eta \text{ id} = \frac{-nE^{\circ}F}{\Delta H}$$

A comparison of the conversion efficiencies shows that for conventional methods, the maximum efficiency to date is about 40 per cent. However, the direct conversion systems appear to have ideal efficiencies of 80 - 100 per cent. Figure 1[3] gives a schematic comparison of the two systems.

One of the direct energy conversion systems receiving much attention is the fuel cell. A fuel cell may be defined [1][5-8] as an electrochemical device in which the chemical energy of a conventional fuel is converted directly, continuously, and usefully, into low-voltage direct-current electrical energy.

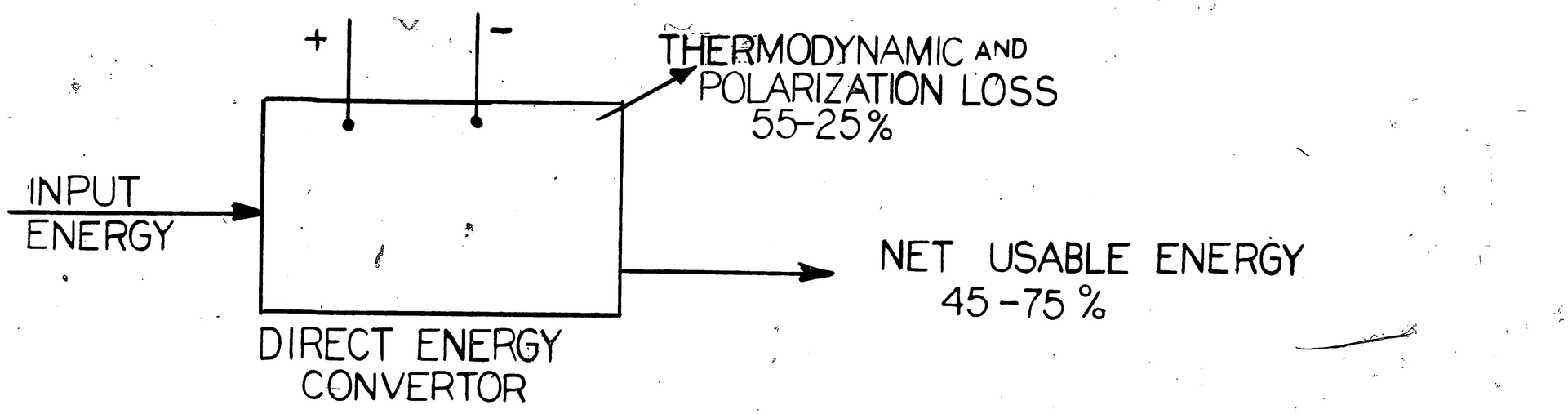

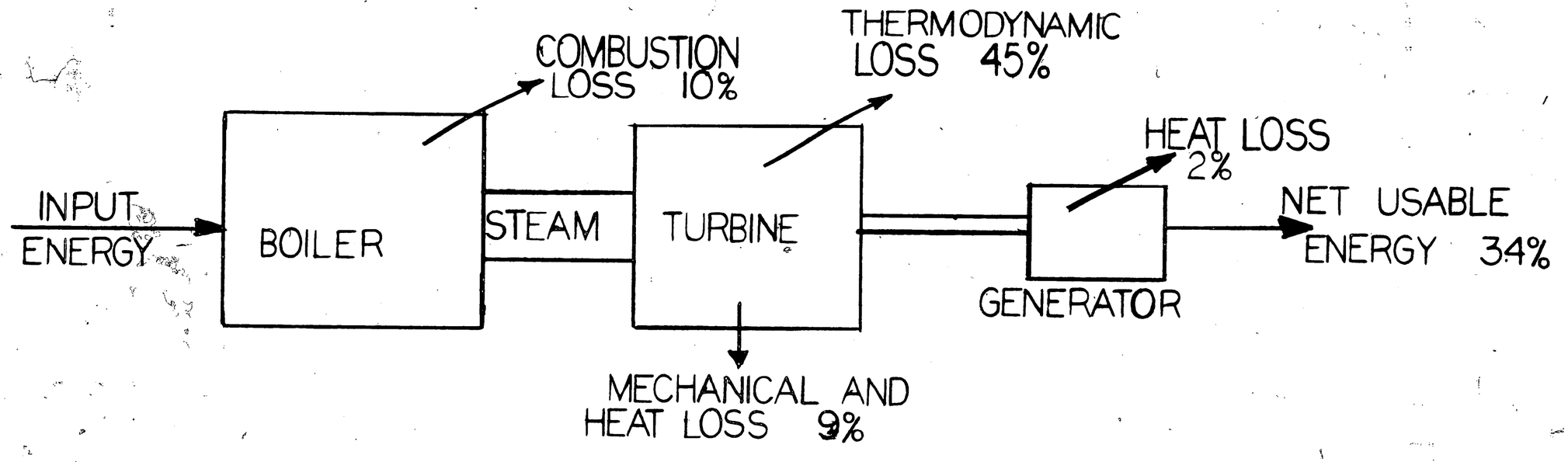

FIGURE 1 - SCHEMATIC COMPARISON OF EFFICIENCIES OF CONVENTIONAL GENERATING EQUIPMENT AND DIRECT ENERGY CONVERSION

Inherent simplicity and high efficiencies make the fuel cell very attractive. There are, however, other advantages which are paramount: (1) Fuel cells are noiseless and have no moving parts, (2) they are clean and generate less heat and toxic fumes than do internal combustion engines, (3) unlike batteries, they do not need recharging, and (4) they have high power per unit volume or weight.

B. HISTORICAL DEVELOPMENT OF FUEL CELLS

The concepts of the fuel cell are not new. As early as 1801 a fuel cell using zinc and oxygen was built by Davy[5]. However, he did not recognise this cell as such. In 1839, Sir William Grove [9], who is considered to be the father of the fuel cell, constructed a chemical battery using platinum catalysts in which the familiar water-forming reaction of hydrogen and oxygen generated an electrical current. However, due to the high cost of platinum, this idea was not followed up. Fifty years later, Mond and Langer[10] developed another version of this device which operated on air or oxygen.

It was not until 1932 when Bacon[7] began working on the idea of fuel cells that any large quantity of research was extended in this area. In 1944, the work towards the development of a practical fuel cell was initiated. Since that time, many industrial firms and institutions have done considerable work in the field of fuel cells. This last

work has been thoroughly covered in many conference proceedings[11-13] and journals.[8][14-16]

C. TYPES OF FUEL CELLS -- CLASSIFICATION

Three types of fuel cells have been under investigation, distinguished largely by their temperature of operation. They are the low-temperature cells which operate in the temperature range from room to 100° C, the medium-temperature cells which operate in the range of 150-250°C, and the high-temperature cells which operate in the range of 500-1000° C.

Considerable success has been obtained in research and development work on the low- and medium-temperature cells in recent years.[11-17] In the medium-temperature category the Bacon cell[7] has reached the highest state of development up to the present. Work has been conducted on the high-temperature fuel cell in several laboratories.[8][11-16]

The low- and medium-temperature cells appear to have a relatively restricted area of application at their present state of development. This is true at least as long as pure hydrogen and oxygen are required as fuel gas and oxidant. It is clear that utilization of relatively impure gases such as water-gas or producer gas, the use of air rather than oxygen, and atmospheric pressure operation would be required before the low-temperature cell could become interesting as a basic power source.

The high-temperature fuel cell has a much larger potential area of application for two reasons: (1) it can accommo-

date relatively cheap fuel gases, and (2) high over-all electrical efficience can be achieved.

The work carried out in this present study was for a low-temperature fuel cell operating with hydrogen as the fuel gas and oxygen as the oxidant.

D. OPERATIONAL FEATURES OF A HYDROGEN-OXYGEN FUEL CELL[3,5,7,17]

Hydrogen and oxygen burn to produce water in order to reach a lower energy state. However, at ordinary temperatures and pressures, additional activation energy is needed to raise the molecules to the energy state at which the reaction will ignite; this energy barrier ordinarily prevents the reaction from proceeding at room temperature. By proper choice of a catalyst, this energy barrier will be lowered and the reaction will proceed rapidly at room temperature. Catalyst selection discussion will be deferred until later.

The cell (Figure 2) consists of two porous electrodes separated by an electrolyte, which in this case is a 27% potassium hydroxide solution. At the fuel electrode or anode, hydrogen gas is fed to the electrode under pressure and diffuses into the electrode. The hydrogen molecules (H_2), assisted by a catalyst embedded in the electrode, are chemisorbed on the internal surface in the form of atomic hydrogen(H). The hydrogen atoms then migrate into the reaction zone (the three-phase boundary between gas, electrolyte, and solid) and react with the hydroxide ions of the electrolyte to form water and release electrons. Summarizing the fuel electrode reactions:

FIGURE 2 - TYPICAL HYDROGEN-OXYGEN FUEL CELL

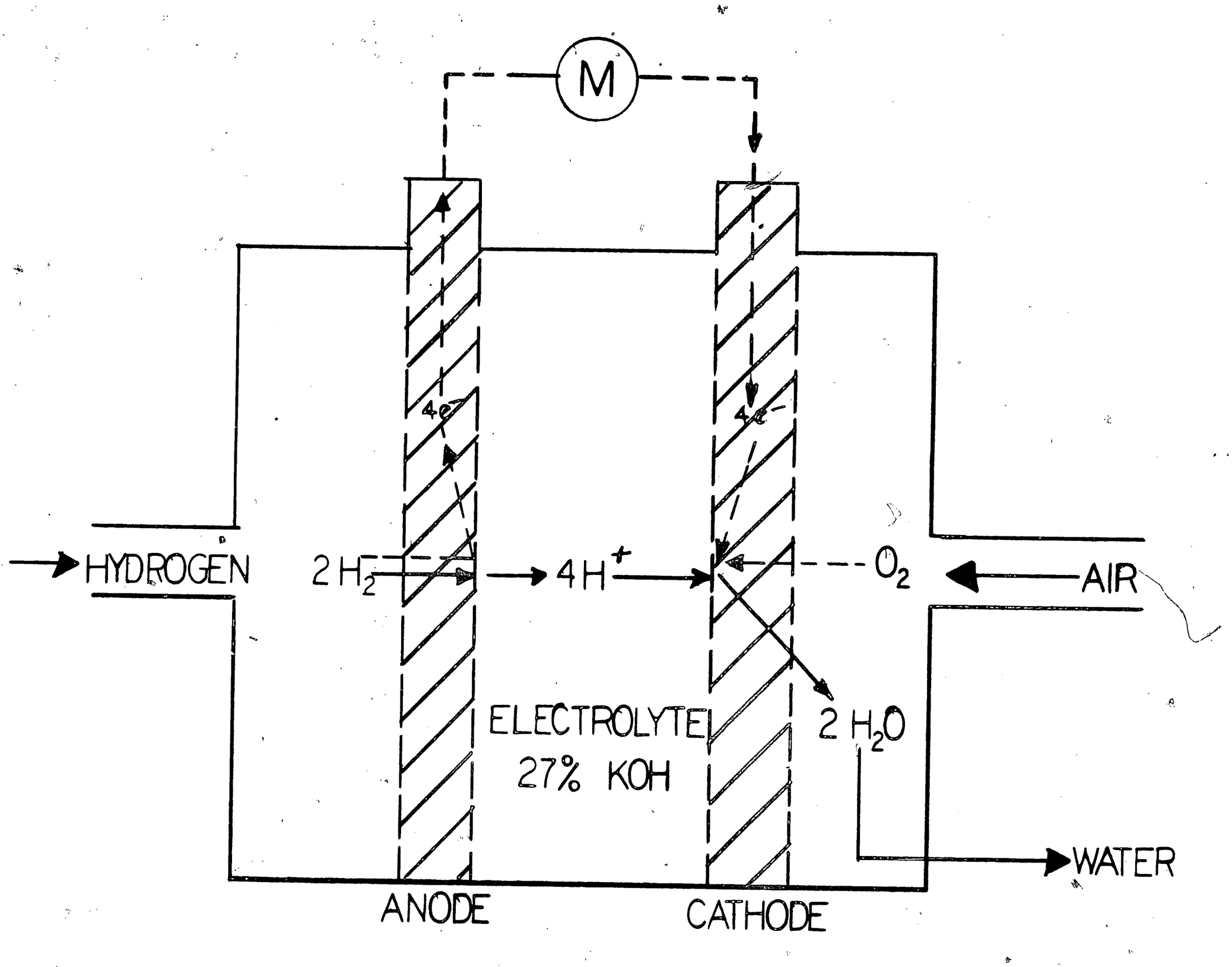

(1) $2H_2$ (free) → $2H_2$ (chemisorbed)

(2) $2\ H_2$ (chemisorbed) → $4H$ (chemisorbed)

(3) $4H$ (chemisorbed) + $4(OH)^-$ → $4\ H_2O + 4e^-$

and the net reaction is:

(4) $2H_2 + 4\ (OH)^- \rightarrow 4H_2O + 4e^-$

After the electrons are released at the fuel electrode, they are conducted through an external circuit where the electrons can perform useful work and then to the oxygen electrode.

At the oxygen electrode or cathode, the molecular oxygen supplied from an external source is introduced into the electrode and is then chemisorbed on a catalytic surface prior to reaction. After chemisorption, the oxygen molecules migrate into the reaction zone of the electrode and combine with the electrons from the fuel electrode and water from the electrolyte to form hydroxyl ions. The hydroxyl ions pass into the electrolyte to replace those consumed concurrently at the hydrogen electrode. Summarizing these reactions:

(5) O_2 (free) → O_2 (chemisorbed)

(6) O_2 (chemisorbed) + $2H_2O + 4e^- \rightarrow 4(OH)^-$

and the net reaction is

(7) O_2 (free) + $2H_2O + 4e^- \rightarrow 4(OH)^-$

The overall cell reaction can now be found by adding reactions (4) and (7):

(4) $2H_2 + 4(OH)^- \rightarrow 4H_2O + 4e^-$

(7) $O_2 + 2H_2O + 4e^- \rightarrow 4(OH)^-$

to give

(8) $2H_2O + O_2 \rightarrow 2\ H_2O$

When the circuit is closed and the resistance across the external circuit between the electrodes is high, the reaction proceeds at a moderate rate, and a high percentage of the reaction energy is released as electricity. Part of the energy is expended at all times in driving the chemical reactions over the barriers of the activation energies of the reactions inside the cell and to overcome internal polarization.

The total polarization[5] of a fuel cell arises from many factors which can be classified into three groups: (1) chemical activation polarization due to energy being consumed in preparing and causing the reactants to electrochemically combine, (2) concentration polarization due to a decrease in the ion and reactant molecule concentration or to an increase in the reaction product concentration, and (3) resistance polarization due to ohmic or electrical resistances to the flow of electrons and ions. It is impossible to measure the actual contribution of every polarization element, but a close approximation can be made by isolating the total polarization losses of each cell element through the use of reference electrodes. By subtracting the total polarization losses from the theoretical cell voltage, the actual cell voltage can be obtained (Figure 3).

FIGURE 3 - SCHEMATIC SHOWING EFFECT OF POLARIZATION LOSSES ON CELL VOLTAGE

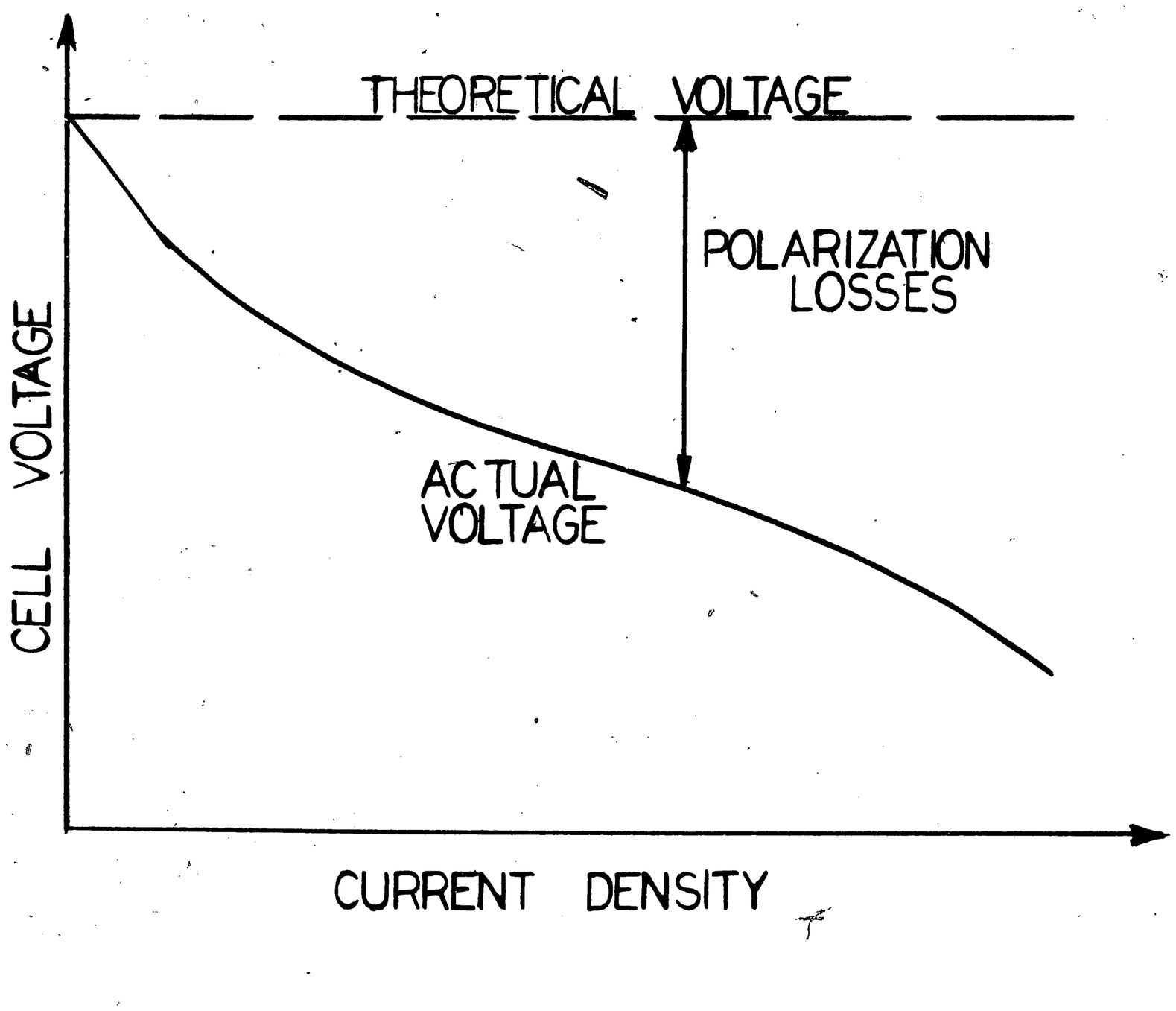

E. ELECTRODES -- DOUBLE SKELETON CATALYST FUEL ELECTRODE

The design of the electrodes for long operating life at high current densities is by far the most serious problem facing fuel-cell workers. Each electrode material, reactant gas, and electrolyte system is unique. In general, a good fuel electrode for use with caustic electrolytes should meet the following requirements:

(a) The activity of the electrode material must be such that it corresponds to that of the most active hydrogenation catalyst known in order to have sufficient hydrogen ion flow at temperatures below 100° C.

(b) The electrode material must have maximum resistance to poisoning.

(c) The material must have mechanical strength to withstand operational pressures to 26,000 psi.

(d) The material must have good electrical conductivity.

(e) The material must permit fabrication with a predetermined porosity.

(f) The material must be lye-proof.

(g) Cost of materials should be as low as possible.

The single-layer double-skeleton-catalyst diffusion electrode developed by Justi[17] meets all of these above requirements. The electrode is fabricated from two materials: Raney nickel powder and nickel carbonyl powder.

Raney nickel powder is the most active hydrogenation catalyst known.[18-20] Not only is it highly active but it is also very insensitive to impurities. The Raney nickel obtained by the method of M. Raney[21-23] is a fine-grained, pyrophoric powder with a large internal surface which is required for catalysts. This catalyst satisfies requirements a, b, and g, but not the others.

In order to overcome these difficulties, a supporting macro-skeleton of nickel carbonly powder is introduced. This macro-skeleton contains the grains of Raney catalyst which form the micro-skeleton and provides the electrical conductivity and mechanical strength which the catalyst lacks. Together, these skeletons provide the pores required for satisfactory operation of the fuel electrode.

F. DEFINITION OF THE PROBLEM

The optimum properties of a fuel electrode may be obtained after empirically establishing many parameters such as the composition of the Raney nickel alloy, its grain size and that of the supporting skeleton, the compacting pressure, the sintering temperature, the sintering time, and the blending ratio of the micro- and macro-skeleton materials. The activation or leaching procedure will also affect the properties of the electrode.

In the work presented here, the object was to study the effect of compacting pressure and sintering temperature on the properties of the electrode. The other parameters were held constant and are given in the section for experimental procedure and technique.

EXPERIMENTAL PROCEDURE AND TECHNIQUE

The electrode selected for study in this thesis was a double-skeleton-catalyst electrode similar to that of Justi[17]. Raney nickel alloy number 2813 was used as the catalyst with Grade B carbonyl nickel powder to provide the supporting skeleton.

Raney alloy number 2813 was procured in fine powder form and had a composition corresponding to 50 weight per cent nickel and 50 weight per cent aluminum. According to the binary constitutional diagram for aluminum and nickel provided by Hansen[24], this alloy should contain two phases: Ni_2Al_3, an intermediate phase of trigonal structure which forms peritectically at 1133° C at a composition of 59.19 weight per cent nickel, and $NiAl_3$, a phase of orthorhombic structure forming peritectically at 854° C and having a singular composition of 42.03 weight per cent nickel (Figure 4).

A. ELECTRODE FABRICATION

In the preparation of the electrodes, the mixture of the Raney alloy with the "B" nickel was the first step. The blending ratio of the powders was one part by weight Raney alloy to two parts by weight "B" nickel. These were mixed in a rotating drum for times of 20 to 40 hours to insure a homogeneous powder for fabricating the electrodes.

This powder mixture was then compacted into electrodes using a stainless steel die (Figure 5). The initial powder thickness in the die was 0.1875 inches for all specimens. This powder was compacted at pressures of approximately

FIGURE 4 - NICKEL-ALUMINUM EQUILIBRIUM DIAGRAM
(AFTER HANSEN)

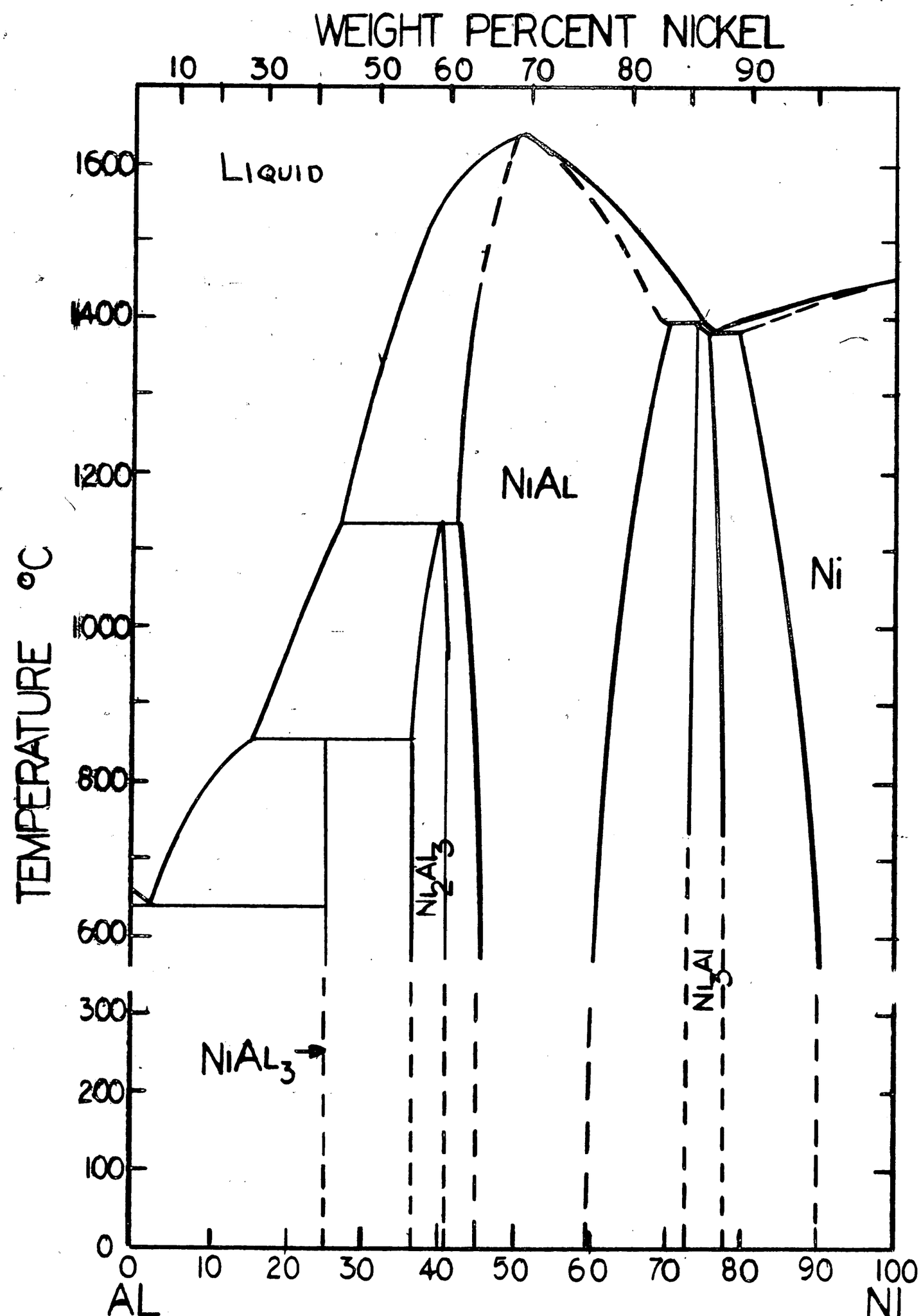

FIGURE 5 - ELECTRODE COMPACTING EQUIPMENT

(TO SCALE)

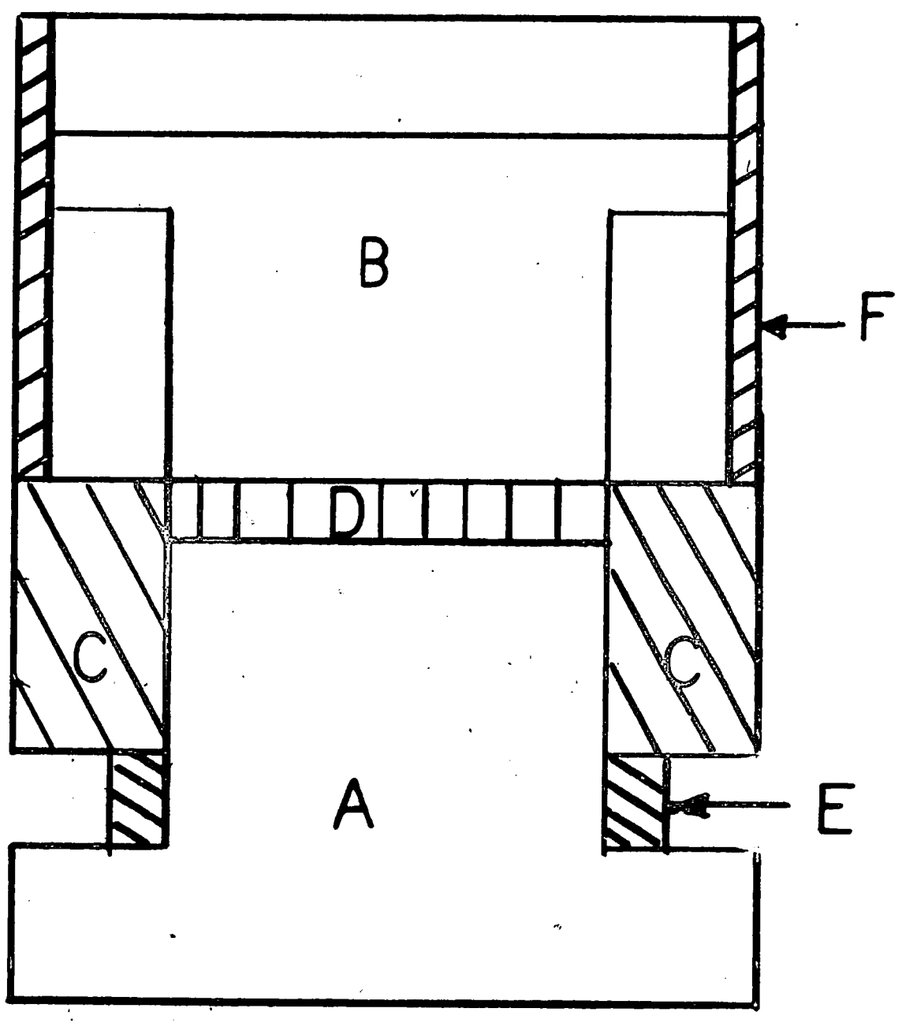

A - BOTTOM DIE
B - TOP DIE
C - CONTAINER
D - ORIGINAL POWDER LEVEL
E - SHIMS
F - BRASS PUSHOUT RING

15,000, 25,000, and 35,000 psi with the force being supplied by a 120,000 pound capacity Baldwin Tensile Testing Machine which was modified to provide compression loads.

Following compacting, each electrode was individually sintered in a resistance-wound furnace capable of handling various atmospheres (Figure 6). The electrodes were placed on graphite pedestals inside the furnace chamber and then the chamber sealed. The electrodes were then heated to sintering temperatures of 750, 775, and 800° C, under a dynamic argon atmosphere. When the electrode had reached the desired temperature, the atmosphere was changed to hydrogen and the specimen was held at temperature for 30 minutes. Then the atmosphere was changed back to argon and the specimen cooled to less than 100° C. Temperature control was maintained by having a chromel-alumel thermocouple inserted into the specimen chamber and maintaining the desired temperature by manually controlling the current in the heating elements.

Following the sintering treatment, each electrode was weighed and its dimensions (diameter and thickness) measured. The electrodes were then ready for activation.

B. ACTIVATION PROCEDURE

Various activation or leaching procedures have been recommended in the literature[20-23][25-31]; however, none of these were duplicated in this work.

Initial activation was carried out on loose Raney alloy powders. The Raney alloy was added to a 6N potassium hydroxide

FIGURE 6

ELECTRODE SINTERING FURNACE

A - Furnace Container

B - Graphite Pedestal

C - Specimen Chamber

D - Atmosphere Inlet

solution which was externally cooled to prevent excessive heating. The hydroxide attacks the aluminum in the alloy and forms an aluminate. The rate of reaction can be followed by observing the evolution of hydrogen which is given off in the leaching process. This reaction was carried out at room temperature while periodically changing the potassium hydroxide solution until no more hydrogen was seen to be evolved. Then the bath was slowly heated to 80° C to permit final activation of the catalyst. During this heating, the potassium hydroxide solution was periodically replenished. X-ray diffraction analysis was made on the "activated" catalyst to determine its structure.

Some of the "activated" catalyst powder was then deactivated by heating in air at temperatures of 75 - 200° C for thirty minutes. Again, X-ray diffraction structural analysis was made.

Another deactivation procedure which was tried was to heat the "activated" catalyst for various lengths of time at the boiling point of 6N potassium hydroxide solution (110-125° C). This temperature was selected because the electrolyte used in the fuel cell is 6N potassium hydroxide solution. However, this test was terminated after almost six hours due to a failure in the deactivation container. X-ray diffraction analysis was made on all specimens to determine the effect of deactivation.

The activation procedure used for the electrodes was not the same as that for the loose powders, in order to compare data with that of the sponsor.

After the electrodes had been sintered, weighed, and their dimensions measured, they were placed in a beaker containing approximately 100 ml. of 1N potassium hydroxide solution for 24 hours. This was exposed to air and the temperature was kept below 50° C. During this 24 hour period, the potassium hydroxide solution was periodically replenished. After this period, the specimens and beakers were placed in a vacuum desiccator which was evacuated for times of 30 to 120 minutes and then sealed off. By using this evacuation procedure, the rate of leaching or activation was increased. Approximately every two days, the vacuum was released and the solutions replenished; after which the chamber was again evacuated. After a month of evacuation in 1N potassium hydroxide solution, the leaching agent was changed to a 27% potassium hydroxide solution. The same evacuation procedure was used. Activation continued until no reaction occurred when fresh leaching solution was added.

C. TEST PROCEDURE

The procedure used for determining the electrical characteristics of each electrode was set up by the Sun Oil Company[32] and used here so that the results could be compared with their data.

After the activation or leaching process was completed, the electrical characteristics of each electrode were determined using the equipment shown in Figures 7 and 8. The electrode was quickly mounted in a teflon test cell and immersed in a 27% potassium hydroxide solution at a temperature of 21 -

FIGURE 7

ELECTRODE TESTING EQUIPMENT

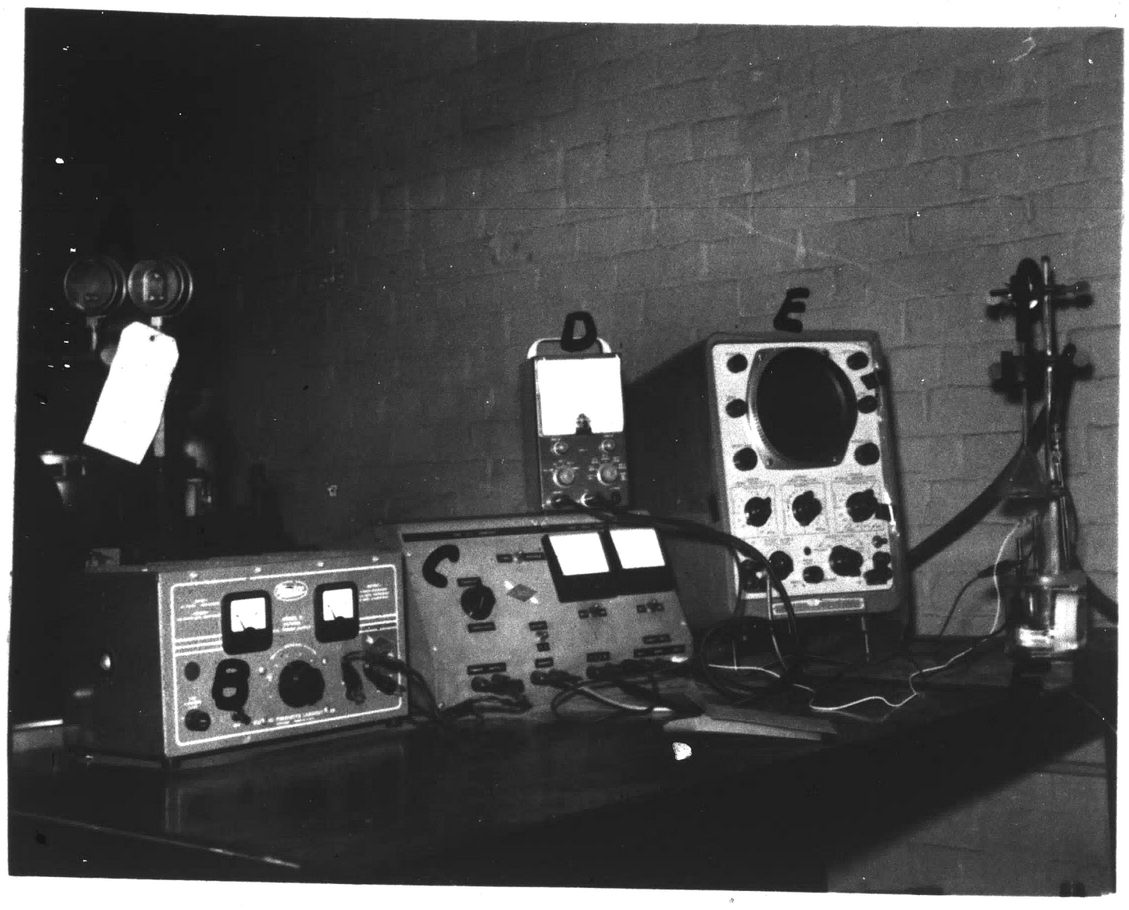

A - Hydrogen Source

B - D. C. Power Supply

C - Ammeters and Current Control

D - Vacuum Tube Voltmeter

E - Oscilloscope

F - Test Cell

FIGURE 8
SPECIMEN HOLDER FOR ELECTRICAL TESTING

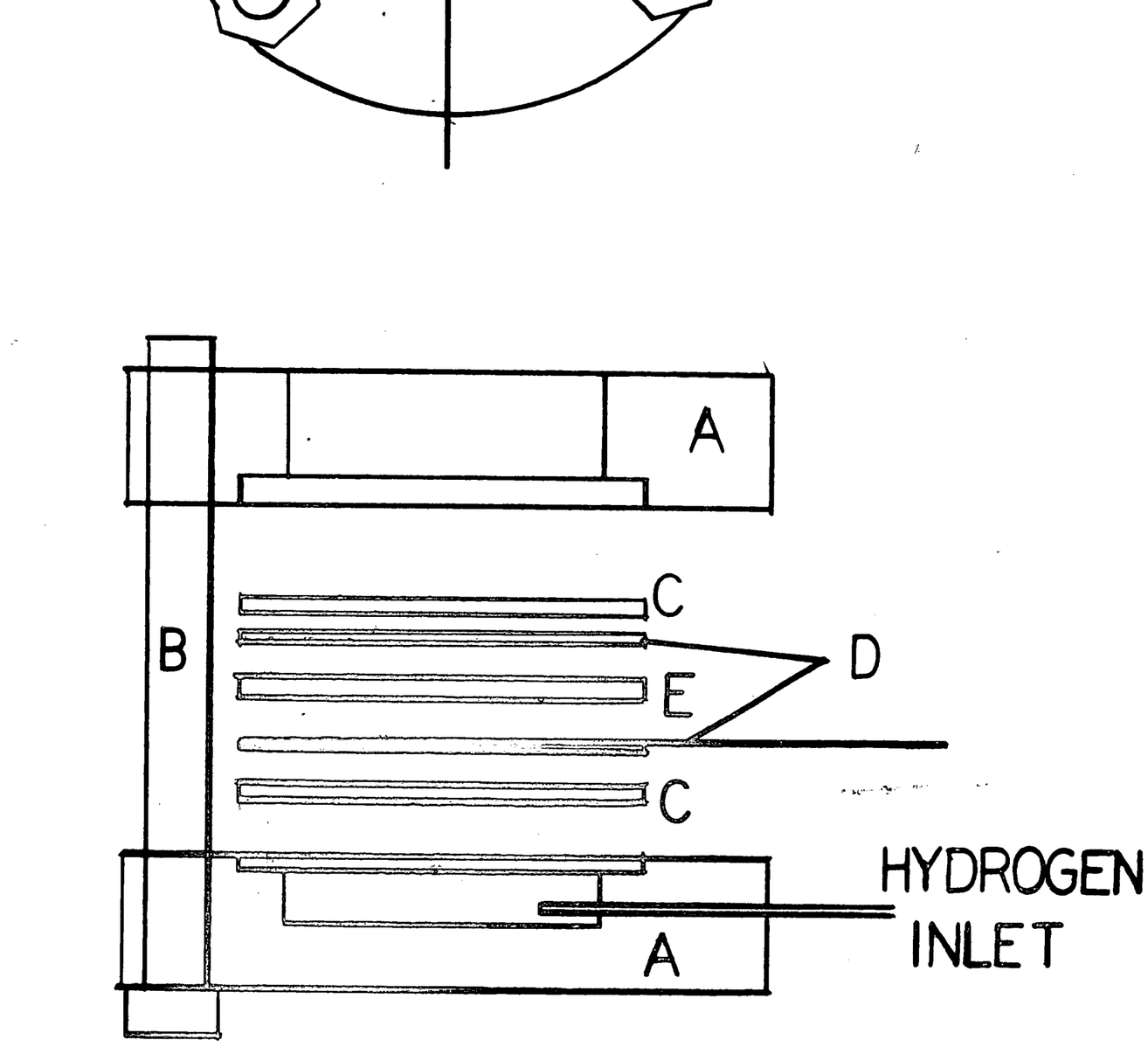

A - TEFLON HOLDER
B - 302 STAINLESS BOLTS
C - RUBBER GASKETS
D - STAINLESS STEEL BACKUP PLATES & PLATINUM ELECTRICAL CONTACT RING
E - DISC ELECTRODE

24° C. The test cell was designed so that hydrogen under pressure could be applied to the back of the electrode while the front was exposed to the electrolyte, similar to the actual fuel cell operation.

The electrode was first purged with hydrogen so that vigorous bubbling of hydrogen occurred on the front side of the electrode and then the hydrogen pressure was reduced to the point where no hydrogen bubbles appeared on the front side of the electrode. The electrode was permitted to remain in this state until the theoretical e.m.f. of the system was reached. Because our reference electrode was Hg-HgO, the theoretical e.m.f. of this half-cell would be 0.93 volts.

When the half-cell had obtained the theoretical e.m.f. at zero load, the load was increased and the electrical characteristics were determined for current densities of 0, 20, 50, 100, 200, and 285 milli-amperes per square centimeter.

The potential was allowed to equilibrate for two minutes at each of the current densities before any measurements were made. At each of the current densities, two measurements were taken:

(1) the e.m.f. of the electrode was read on a Vacuum Tube Voltmeter, and

(2) the IR-drop was read on an oscilloscope.

These two voltages were added together in such a manner as to correct the actual e.m.f. towards the theoretical e.m.f. of 0.93 volts.

After the last measurement was taken, the current density was reduced to zero and the cell was permitted to equilibrate for thirty minutes. During this period, the e.m.f. read on the Vacuum Tube Voltmeter returned to the theoretical e.m.f.

Then the current density was increased to a constant value of 70 milli-amperes per square centimeter and the electrical characteristics were determined as a function of time at constant current density. Cell e.m.f. and IR-drop readings were made at 0, 5, 10, 15, 20, and 30 minutes. The data were handled in the same manner as before. After testing was completed, the electrodes were stored in 1N potassium hydroxide solution.

Because the measurements require a constant power supply, the load on the cell was a direct current supplied by an Electro Model B Filtered D.C. Power Supply.

D. X-RAY DIFFRACTION ANALYSIS

Powder examination was performed on a G.E. XRD-4 diffraction apparatus with associated G.E. cameras and accessories. The diameter of the G.E. camera was 14.32 cm.

Spindles were prepared using Pyrex glass in the form of drawn fibers of about 0.005 inch diameter; the absorption was found negligible and the glass itself was found non-diffracting. The powder was applied to the spindle using a bonding agent of collodion thinned to the desired viscosity with amyl acetate.

Concentricity of rotation in the G.E. camera was assured by observing the rotation of the spindle in the slit image formed on a white background after passing light through the collimator from its tube side.

Kodak Medical No-Screen film was used for recording diffraction data. Film processing was performed in Kodak X-ray developing and fixing solutions for the times at temperatures recommended. Films were washed a minimum of three hours and allowed to dry for 24 to 48 hours in still air before measurement.

Electrode examination was performed on a Siemens Crystalloflex IV diffraction unit using a scintillation counter and a direct recording device to record the diffraction data. A special holder was constructed to permit the use of a whole electrode in the diffraction studies.

RESULTS

A. RESULTS OF ELECTRODE TESTING

Electrodes produced from a powder mixture of one part by weight Raney alloy and two parts by weight "B" nickel were fabricated according to the procedure previously outlined. The actual fabrication data (compacting pressure and sintering temperature) are given in Table I together with the size and weight of the electrode after sintering. The electrodes were then activated and tested by the previously mentioned procedures. Results of these tests are given in Tables II-A to II-P.

It had been determined that the theoretical open-circuit voltage of the hydrogen half-cells being tested should be 0.93 volts when using a mercury-mercuric oxide reference electrode. In all tests, the e.m.f. of the cell approached this value before any load was applied.

Upon application of a load, the e.m.f. of the cell should become less than this theoretical value due to the polarization losses. With the present testing system, it is possible to determine the ohmic polarization of the cell and thus get an idea of the magnitude of the activation and concentration polarizations. This latter could be obtained by correcting the actual e.m.f. of the cell back towards the theoretical, the difference between the corrected e.m.f. and the theoretical being due to activation and concentrations.

Table I - Electrode Fabrication Data

Material: 1 part Raney Catalyst No. 2813 to 2 parts "B" nickel

Original Thickness: 3/16" for all Specimens

Electrode	Compacting Pressure (a)	Sintering Temperature	Weight (b)	Diameter (b)	Thickness (b)
DM1-1	15,220psi	791±5°C	8.8315 g	1.512 in.	0.0965 in.
DM1-2	15,280	775±5	9.2964	1.4945	0.09725
DM1-3	15,220(c)	750±5	8.6475	1.4827	0.0875
DM2-1	24,960	795±5	7.1625	1.505	0.070
DM2-2	24,960(d)	775±5	6.6548	1.4773	0.061
DM2-3	24,960	750±5	6.5132	1.4775	0.060
DM2-4	25,020	775±5	6.6484-	1.486	0.062
DM2-5	35,160	800±5	6.8968	1.484	0.061
DM2-6	35,220	775±5	6.4770	1.4855	0.057
DM2-7	35,200	750±5	6.5130	1.483	0.057
DM2-8	15,010	750±5	7.5762	1.4985	0.0785
DM2-9	14,410	750±5	7.3135	1.4987	0.0725
DM2-10	28,730	775±5	7.2303	1.484	0.0672
DM2-11	24,970	750±5	7.2972	1.481	0.0675
DM2-12	34,980	800±5	7.3675	1.478	0.0637
DM2-13	34,990	775±5	7.3473	1.4815	0.0648

(a) Pressure based on initial area.
(b) Measured after sintering.
(c) Pressure jumped to 16,700 psi at end of cycle.
(d) Pressure jumped to 28,700 psi at end of cycle.

Table II-A. Electrode Testing Data for DM1-1

1. Test at Constant Time (2 minutes)

Current Density	IR Drop	Corrected EMF
0 ma/cm²	0.0 volts	0.91 volts
20	0.185	0.905
50	0.235	0.875
100	0.375	0.875
200	0.68	0.88
285	0.74	0.740

2. Test at Constant Current Density (70 ma/cm²)

Time	IR Drop	Corrected EMF
0 min.	0.044 volts	0.884 volts
5	0.260	0.79
10	0.285	0.755
15	0.31	0.73
20	0.33	0.69
30	0.375	0/595

Table II-B. Electrode Testing Data for DM1-2

1. Test at Constant Time (2 minutes)

Current Density	IR Drop	Corrected EMF
0 ma/cm^2	0.0 volts	0.93 volts
20	0.095	0.895
50	0.22	0.88
100	0.35	0.885
200	0.53	0.865
285	0.61	0.72

2. Test at Constant Current Density (70 ma/cm^2)

Time	IR Drop	Corrected EMF
0 min.	0.040 volts	0.909 volts
5	0.235	0.84
10	0.235	0.81
15	0.235	0.79
20	0.240	0.77
30	0.235	0.715

Table II-C. Electrode Testing Data for DM1-3

1. Test at Constant Time (2 minutes)

Current Density	IR Drop	Corrected EMF
0 ma/cm²	0.0 volts	0.92 volts
20	0.54	1.08
50	0.54	1.00
100	0.60	0.95
200	0.74	0.90
285	0.84	0.79

2. Test at Constant Current Density (70 ma/cm²)

Time	IR Drop	Corrected EMF
0 min.	0.0 volts	0.86 volts
5 min	0.48	0.86
10	0.47	0.86
15	0.45	0.815
20	0.46	0.80
30	0.46	0.75

Table II-D. Electrode Testing Data for DM2-1

1. Test at Constant Time (2 minutes)

Current Density	IR Drop	Corrected EMF
0 ma/cm²	0.0 volts	0.92 volts
20	0.041	0.886
50	0.112	0.882
100	0.240	0.89
200	0.58	0.88
285	0.62	0.85

2. Test at Constant Current Density (70 ma/cm²)

Time	IR Drop	Corrected EMF
0 min.	0.040 volts	0.90 volts
5	0.13	0.82
10	0.135	0.79
15	0.135	0.745
20	0.14	0.705
30	0.15	0.59

Table II-E. Electrode Testing Data for DM2-2

1. Test at Constant Time (2 minutes)

Current Density	IR Drop	Corrected EMF
0 ma/cm²	0.0 volts	0.925 volts
20	0.29	0.93
50	0.42	0.93
100	0.50	0.93
200	0.64	0.92
285	0.80	0.89

2. Test at Constant Current Density (70 ma/cm²)

Time	IR Drop	Corrected EMF
0 min.	0.0 volts	0.91 volts
5	0.52	0.92
10	0.43	0.89
15	0.47	0.90
20	0.47	0.87
30	0.40	0.81

Test II-F. Electrode Testing Data for DM2-3

1. Test at Constant Time (2 minutes)

Current Density	IR Drop	Corrected EMF
0 ma/cm²	0.0 volts	0.925 volts
20	0.30	0.95
50	0.43	0.93
100	0.47	0.91
200	0.60	0.88
285	0.69	0.79

2. Test at Constant Current Density (70 ma/cm²)

Time	IR Drop	Corrected EMF
0 min	0.0 volts	0.89 volts
5	0.245	0.85
10	0.24	0.815
15	0.265	0.80
20	0.285	0.78
30	0.305	0.71

Table II-G. Electrode Testing Data for DM2-4

1. Test at Constant Time (2 minutes)

Current Density	IR Drop	Corrected EMF
0 ma/cm²	0.0 volts	0.925 volts
20	0.26	0.90
50	0.35	0.92
100	0.45	0.93
200	0.58	0.90
285	0.66	0.815

2. Test at Constant Current Density (70 ma/cm²)

Time	IR Drop	Corrected EMF
0 min.	0.015 volts	0.93 volts
5	0.19	0.825
10	0.195	0.80
15	0.20	0.775
20	0.20	0.765
30	0.20	0.725

Table II-H. Electrode Testing Data for DM2-5

1. Test at Constant Time (2 minutes)

Current Density	IR Drop	Corrected EMF
0 ma/cm²	0.0 volts	0.93 volts
20	0.37	0.975
50	0.44	0.96
100	0.54	0.96
200	0.65	0.92
285	0.72	0.78

2. Test at Constant Current Density (70 ma/cm²)

Time	IR Drop	Corrected EMF
0 min.	0.075 volts	0.925 volts
5	0.19	0.835
10	0.195	0.815
15	0.195	0.785
20	0.20	0.76
30	0.205	0.73

Table II-I. Electrode Testing Data for DM2-6

1. Test at Constant Time (2 minutes)

Current Density	IR Drop	Corrected EMF
0 ma/cm²	0.0 volts	0.93 volts
20	0.265	0.945
50	0.38	0.94
100	0.54	0.96
200	0.80	0.92
285	0.92	0.84

2. Test at Constant Current Density (70 ma/cm²)

Time	IR Drop	Corrected EMF
0 min.	0.0 volts	0.92 volts
5	0.225	0.835
10	0.23	0.815
15	0.23	0.785
20	0.23	0.775
30	0.235	0.735

Table II-J. Electrode Testing Data for DM2-7

1. Test at Constant Time (2 minutes)

Current Density	IR Drop	Corrected EMF
0 ma/cm²	0.0 volts	0.92 volts
20	0.025	0.865
50	0.075	0.85
100	0.215	0.865
200	0.37	0.845
285	0.46	0.785

2. Test at Constant Current Density (70 ma/cm²)

Time	IR Drop	Corrected EMF
0 min.	0.0 volts	0.95 volts
5	0.12	0.84
10	0.125	0.82
15	0.13	0.80
20	0.13	0.79
30	0.13	0.76

Table II-K. Electrode Testing Data for DM2-8

1. Test at Constant Time (2 minutes)

Current Density	IR Drop	Corrected EMF
0 ma/cm²	0.030 volts	0.93 volts
20	0.225	0.925
50	0.305	0.915
100	0.48	0.92
200	0.73	0.91
285	0.86	0.85

2. Test at Constant Current Density (70 ma/cm²)

Time	IR Drop	Corrected EMF
0 min.	0.0 volts	0.905 volts
5	0.43	0.90
10	0.46	0.86
15	0.47	0.79
20	0.46	0.71
30	0.47	0.57

Table II-L. Electrode Testing Data for DM2-9

1. Test at Constant Time (2 minutes)

Current Density	IR Drop	Corrected EMF
0 ma/cm²	0.030 volts	0.93 volts
20	0.050	0.89
50	0.24	0.92
100	0.32	0.905
200	0.46	0.91
285	0.56	0.88

2. Test at Constant Current Density (70 ma/cm²)

Time	IR Drop	Corrected EMF
0 min.	0.035 volts	0.905 volts
5	0.305	0.89
10	0.33	0.875
15	0.325	0.855
20	0.325	0.845
30	0.325	0.82

Table II-M. Electrode Testing Data for DM2-10

1. Test at Constant Time (2 minutes)

Current Density	IR Drop	Corrected EMF
0 ma/cm²	0.030 volts	0.935 volts
20	0.029	0.899
50	0.064	0.879
100	0.124	0.874
200	0.25	0.88
285	0.33	0.82

2. Test at Constant Current Density (70 ma/cm²)

Time	IR Drop	Corrected EMF
0 min.	0.030 volts	0.935 volts
5	0.09	0.86
10	0.09	0.845
15	0.091	0.826
20	0.094	0.799
30	0.094	0.749

Table II-N. Electrode Testing Data for DM2-11

1. Test at Constant Time (2 minutes)

Current Density	IR Drop	Corrected EMF
0 ma/cm²	0.018 volts	0.922 volts
20	0.037	0.889
50	0.100	0.882
100	0.225	0.897
200	0.57	0.862
285	0.70	0.732

2. Test at Constant Current Density (70 ma/cm²)

Time	IR Drop	Corrected EMF
0 min.	0.026 volts	0.926 volts
5	0.195	0.86
10	0.195	0.82
15	0.195	0.79
20	0.195	0.77
30	0.195	0.715

Table II-0. Electrode Testing Data for DM2-12

1. Test at Constant Time (2 minutes)

Current Density	IR Drop	Corrected EMF
0 ma/cm²	0.030 volts	0.93 volts
20	0.064	0.899
50	0.21	0.915
100	0.315	0.915
200	0.43	0.885
285	0.59	0.84

2. Test at Constant Current Density (70 ma/cm²)

Time	IR Drop	Corrected EMF
0 min.	0.0 volts	0.92 volts
5	0.15	0.87
10	0.15	0.83
15	0.15	0.815
20	0.15	0.79
30	0.15	0.745

Table II-P. Electrode Testing Data for DM2-13

1. Test at Constant Time (2 minutes)

Current Density	IR Drop	Corrected EMF
0 ma/cm²	0.030 volts	0.93 volts
20	0.032	0.887
50	0.084	0.859
100	0.19	0.92
285	0.76	0.93

2. Test at Constant Current Density (70 ma/cm²)

Time	IR Drop	Corrected EMF
0 min.	0.0 volts	0.915 volts
5	0.108	0.868
10	0.116	0.841
15	0.138	0.828
20	0.143	0.818
30	0.145	0.73

The corrected e.m.f. is found by adding the ohmic polarization to the measured e.m.f. in a manner mentioned above.

It can be noted from the data that electrodes DM1-3, DM2-3, DM2-5, and DM2-6 gave results for the corrected e.m.f. which were larger than the theoretical open-circuit e.m.f. This could be due in part to either experimental error or fluctuations in the line voltage. However, it is felt that these anomalous results are due to incomplete activation; that is, all of the aluminum had not been removed from the electrode and thus gave rise to higher voltages.

Another anomaly in the data appears in the tests at constant current density where the ohmic polarization should range between that observed for 50 milli-amperes per square centimeter and 100 milli-amperes per square centimeter in the constant time tests. Electrodes DM1-3, DM2-3, DM2-4, DM2-5, and DM2-6 all show ohmic polarization losses in the constant current density test which are lower than that expected from the constant time tests. Most of these electrodes also showed previously noted discrepancies which are probably due to incomplete activation.

In an effort to analyze for these discrepancies, two approaches were taken: (1) retest the electrodes after they had been stored for several weeks in 1N potassium hydroxide solution, and (2) make up new electrodes, duplicating the fabrication procedures of the electrodes in question. The new electrodes are labeled DM2-8 to DM2-13 inclusive and correspond to the original electrodes as follows:

DM1-3 - - - - DM2-8 and DM2-9

DM2-3 - - - - DM2-11

DM2-5 - - - - DM2-12

DM2-6 - - - - DM2-13

The results of these electrodes are given in Tables II-K to II-P.

In all the tests at constant time, the results showed that activation had apparently been complete as all corrected e.m.f. values were below the theoretical e.m.f. Electrode DM2-13 showed highly irregular results which cannot be explained. The results of the constant current density tests showed that the ohmic polarizations for all electrodes except DM2-12 were in agreement with that expected from the constant time tests.

The data of the retests are given in Tables III-A to III-D. The results indicate that the catalyst has deteriorated with time but that activation was apparently completed during the storage period. This deterioration agrees with the results of Smith, Bedoit, and Fuzek[17]. However, the constant current density tests still indicate ohmic polarizations less than that expected from the constant time tests.

The data for the constant time tests indicated (Figures 9A,B,C, and 10A,B,C) that the best results were obtained from the electrodes compacted at 15,000 or 25,000 psi and sintered at 750 or 775° C. The higher the compacting pressure, the higher the sintering temperature, or a combination of both, the less porous will be the resulting electrode. Since the

Table III-A. Retest Data for DM1-3

1. Test at Constant Time (2 minutes)

Current Density	IR Drop	Corrected EMF
0 ma/cm²	0.0 volts	0.91 volts
20	0.082	0.92
50	0.20	0.875
100	0.25	0.81
200	0.30	0.63
285	0.34	0.44

2. Test at Constant Current Density (70 ma/cm²)

Time	IR Drop	Corrected EMF
0 min	0.0 volts	0.92 volts
5	0.096	0.781
10	0.096	0.711
15	0.096	0.621
20	0.096	0.516
30	0.098	0.343

Table III-B. Retest Data for DM2-3

1. Test at Constant Time (2 minutes)

Current Density	IR Drop	Corrected EMF
0 ma/cm²	0.0 volts	0.92 volts
20	0.023	0.883
50	0.068	0.828
100	0.14	0.755
200	0.29	0.45
285	0.36	0.0

2. Test at Constant Current Density (70 ma/cm²)

Electrode failed to return to theoretical voltage

- test discontinued

Table III-C. Retest Data for DM2-4

1. Test at Constant Time (2 minutes)

Current Density	IR Drop	Corrected EMF
0 ma/cm²	0.0 volts	0.935 volts
20	0.025	0.905
50	0.07	0.855
100	0.144	0.809
200	0.29	0.76
285	0.39	0.59

2. Test at Constant Current Density (70 ma/cm²)

Time	IR Drop	Corrected EMF
0 min.	0.0 volts	0.92 volts
5	0.105	0.77
10	0.105	0.665
15	0.105	0.525
20	0.110	0.39
30	0.115	0.135

Table III-D. Retest Data for DM2-5

1. Test at Constant Time (2 minutes)

Current Density	IR Drop	Corrected EMF
0 ma/cm²	0.0 volts	0.927 volts
20	0.102	0.907
50	0.242	0.892
100	0.412	0.892
200	0.612	0.867
285	0.722	0.722

2. Test at Constant Current Density (70 ma/cm²)

Time	IR Drop	Corrected EMF
0 min.	0.0 volts	0.915 volts
5	0.16	0.825
10	0.16	0.80
15	0.16	0.77
20	0.16	0.745
30	0.16	0.68

FIGURE 9A - COMPARISON OF CURRENT DENSITY DATA FOR ELECTRODES COMPACTED AT 15000 PSI AND SINTERED AT VARIOUS TEMPERATURES

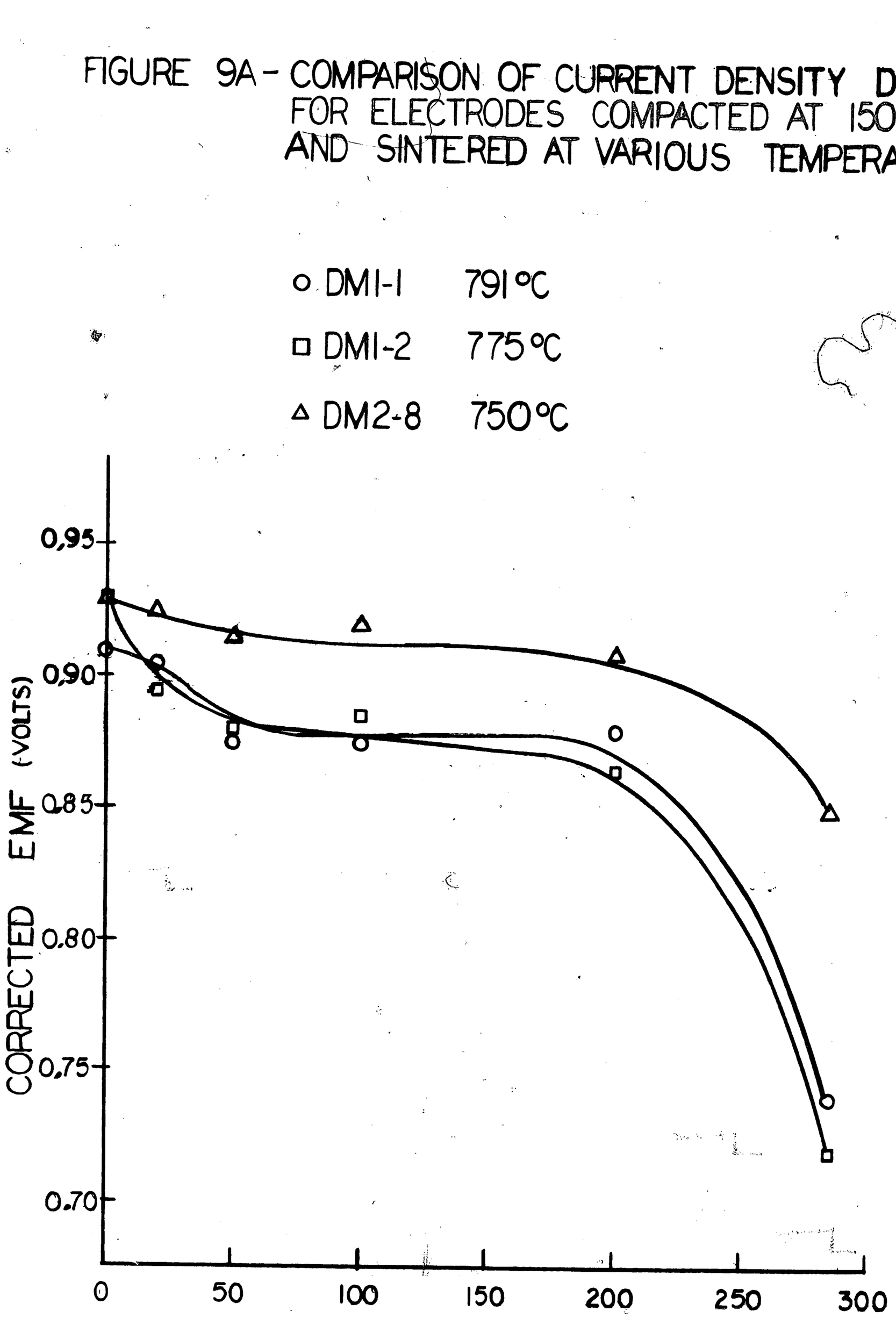

FIGURE 9B - COMPARISON OF CURRENT DENSITY DATA FOR ELECTRODES COMPACTED AT 25000 PSI AND SINTERED AT VARIOUS TEMPERATURES

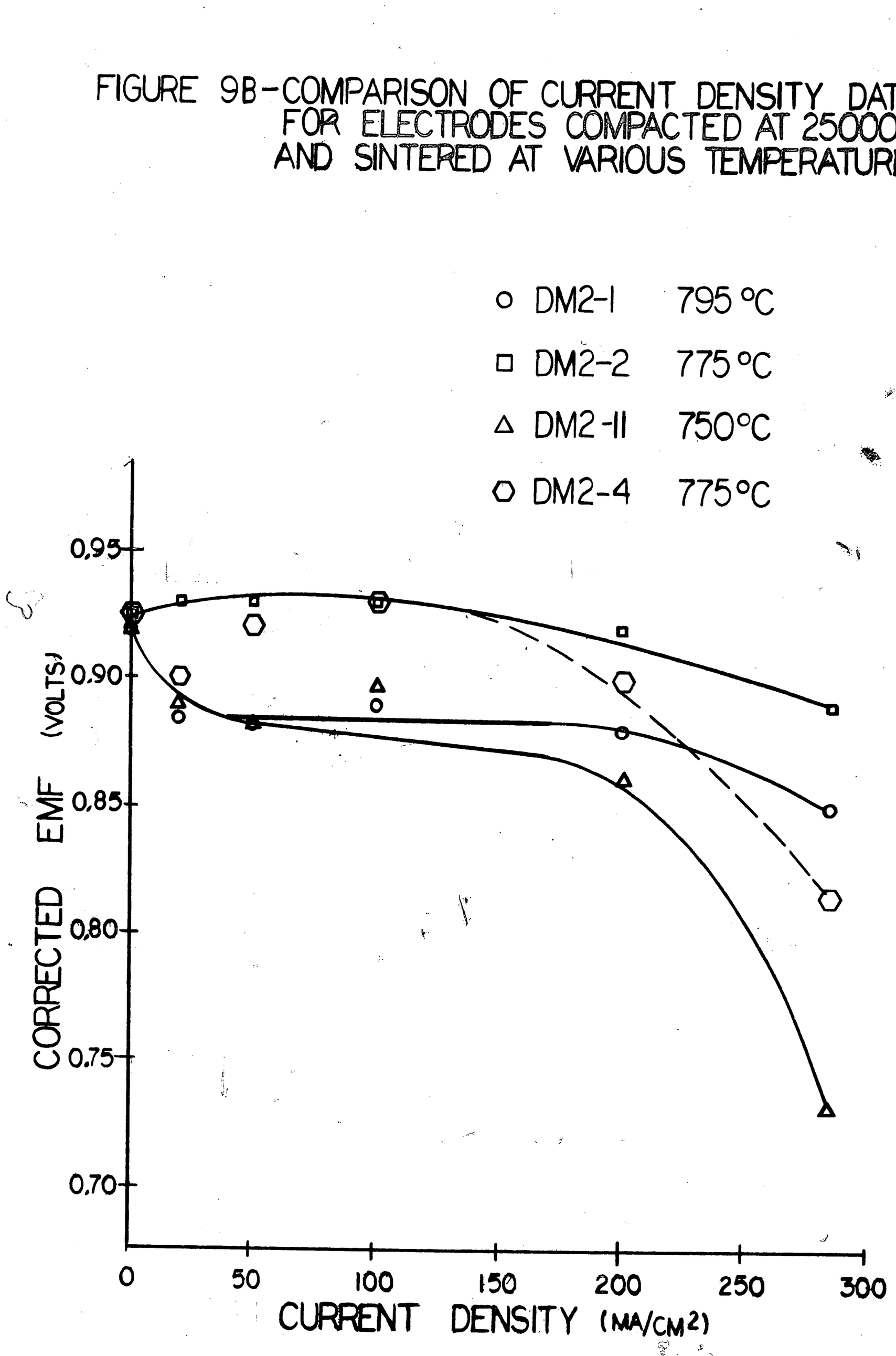

FIGURE 9C - COMPARISON OF CURRENT DENSITY DATA FOR ELECTRODES COMPACTED AT 35000 PSI AND SINTERED AT VARIOUS TEMPERATURES

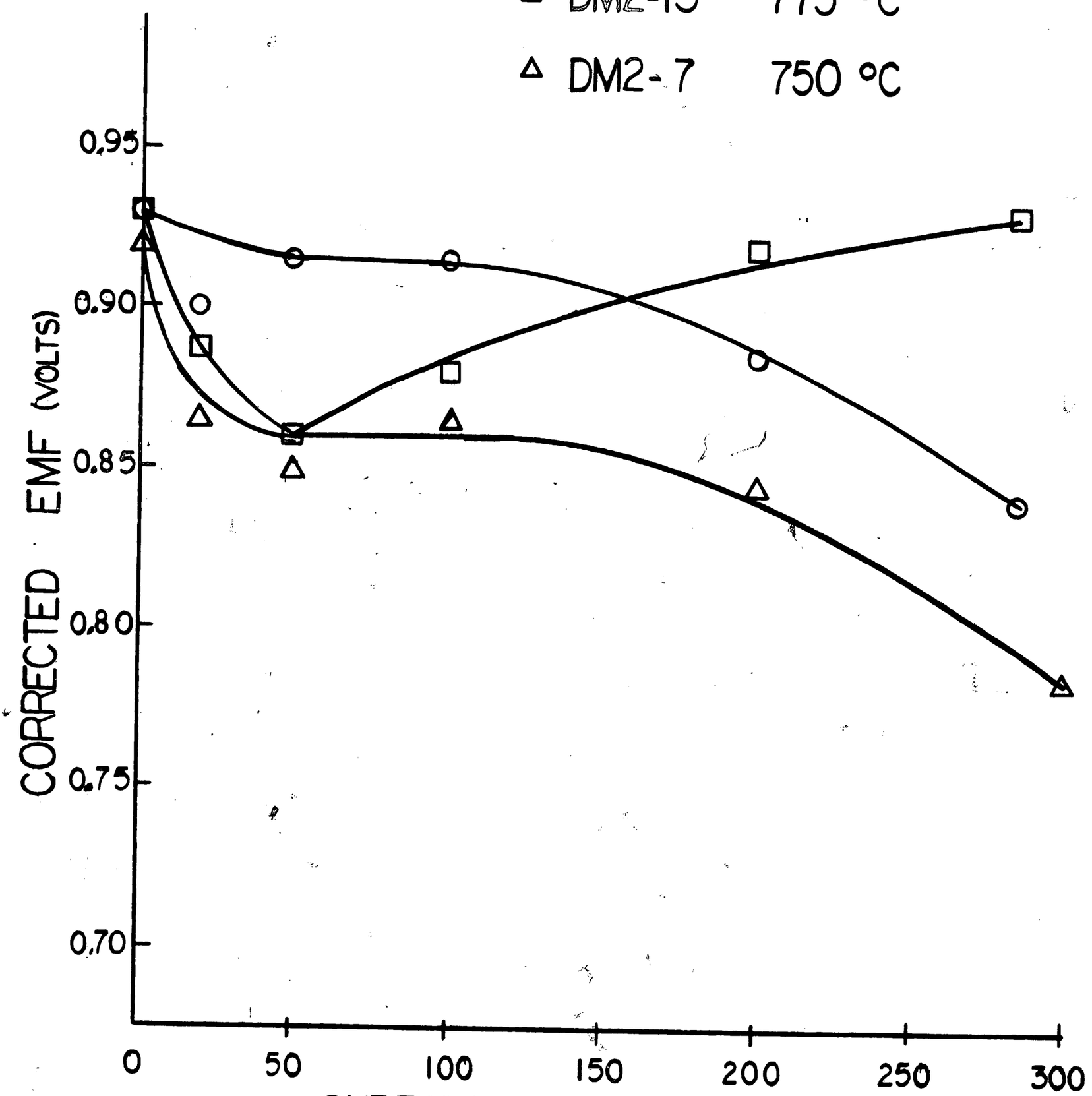

FIGURE 10A - COMPARISON OF CURRENT DENSITY DATA FOR ELECTRODES SINTERED AT 750 °C AND COMPACTED AT VARIOUS PRESSURES

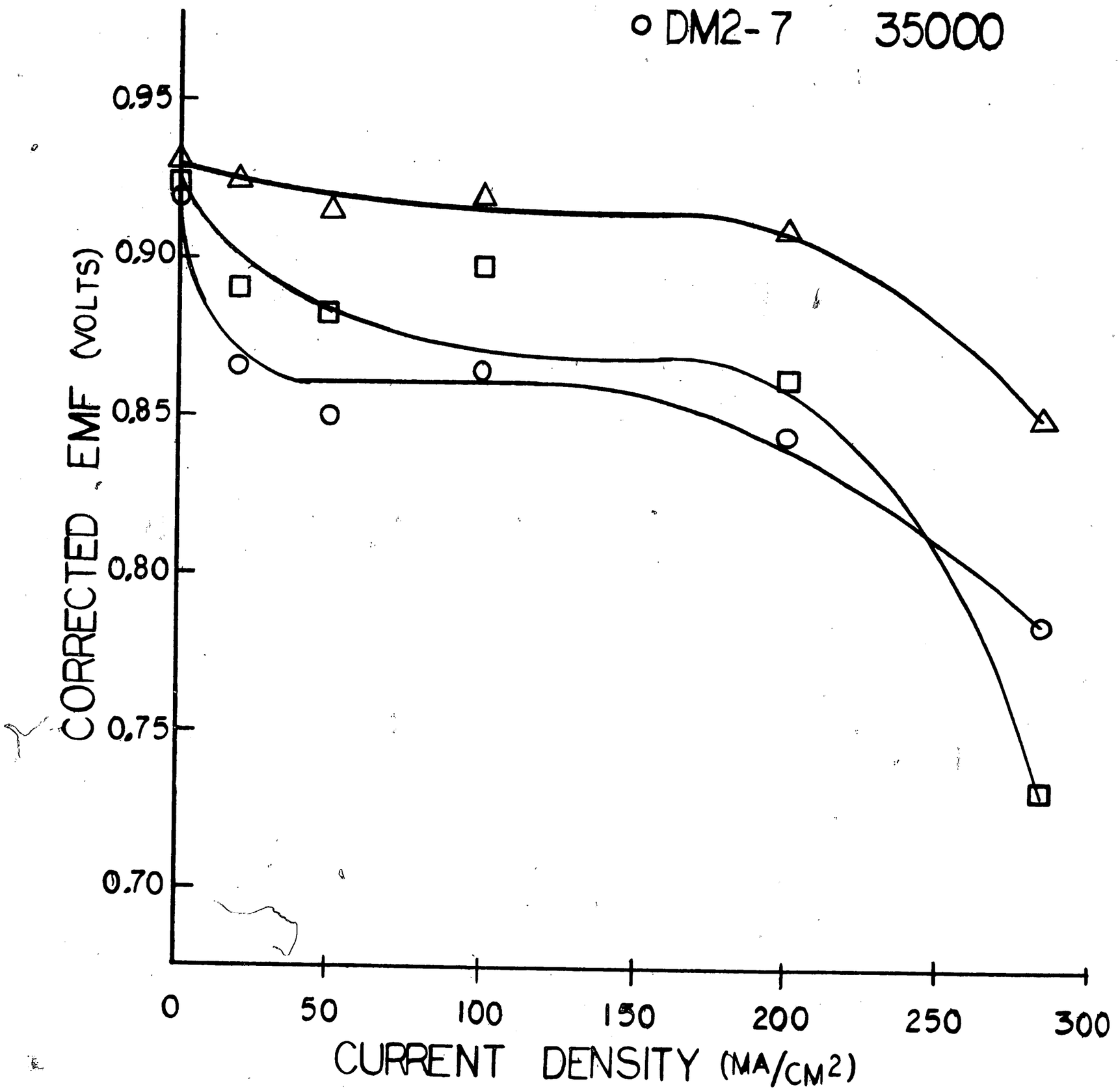

FIGURE 10B - COMPARISON OF CURRENT DENSITY DATA FOR ELECTRODES SINTERED AT 775°C AND COMPACTED AT VARIOUS PRESSURES

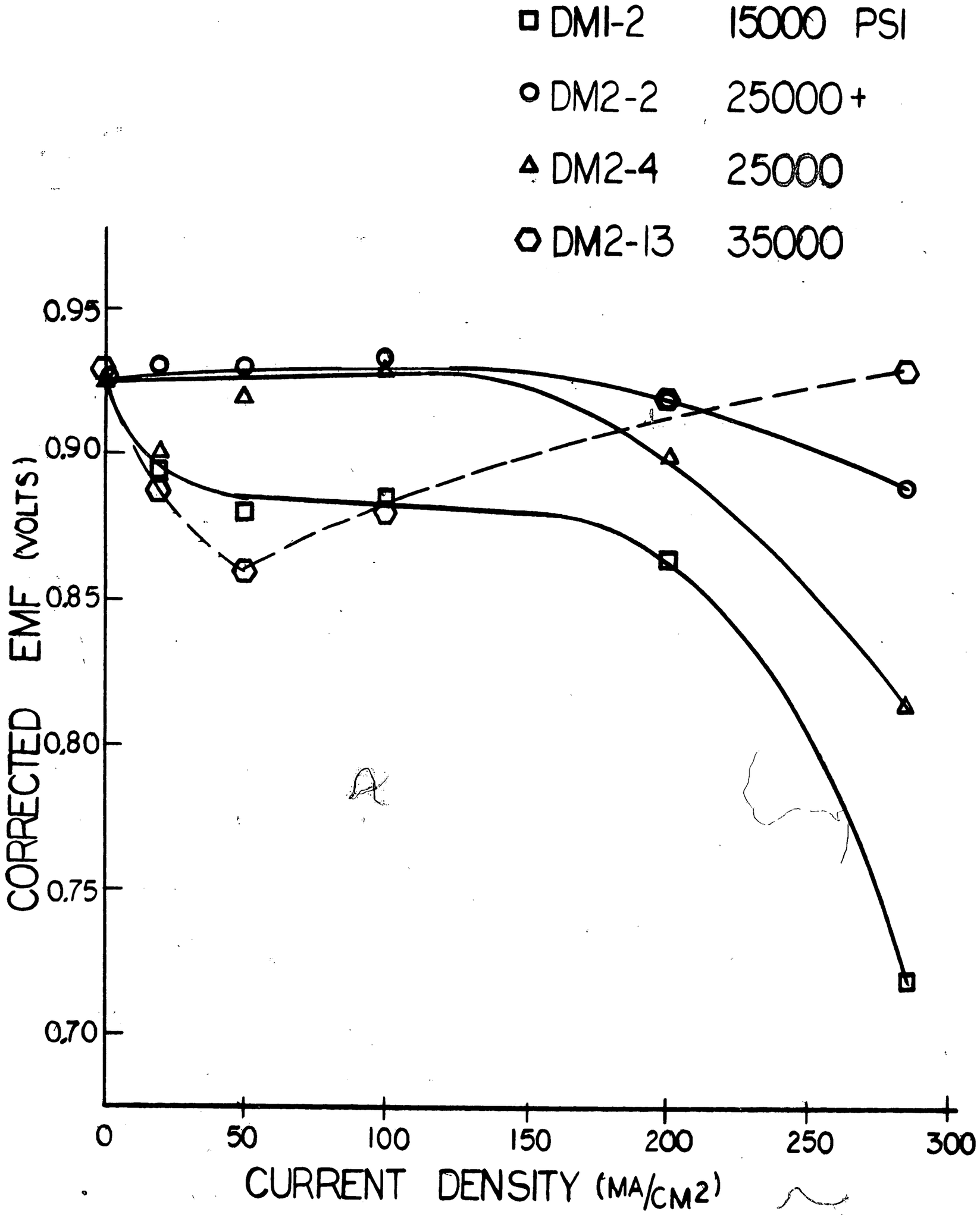

FIGURE 10C-COMPARISON OF CURRENT DENSITY DATA FOR ELECTRODES SINTERED AT 795 °C AND COMPACTED AT VARIOUS PRESSURES

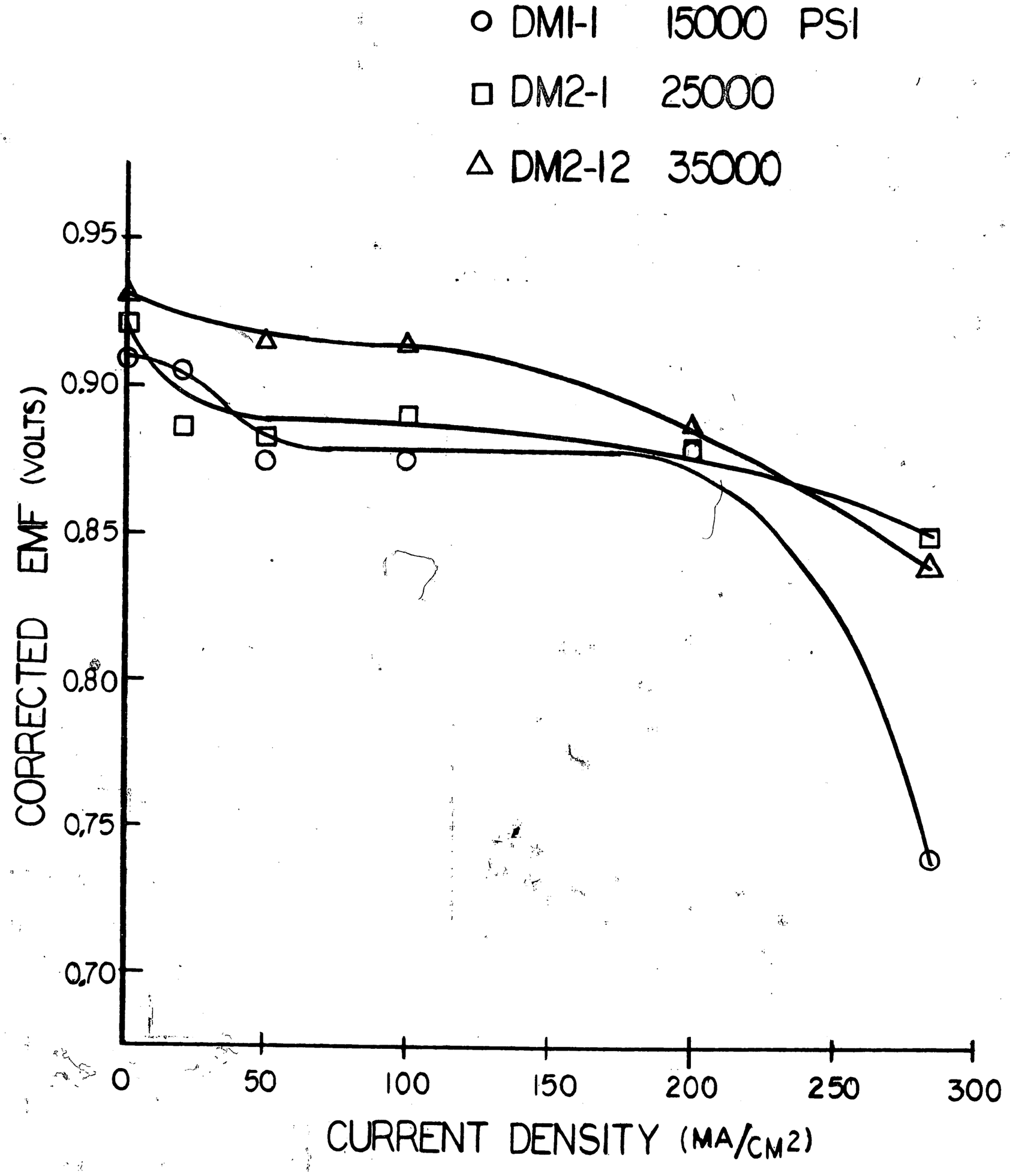

successful operation of the fuel electrode depends on a certain amount of porosity, one would conclude that lower compacting pressures and lower sintering temperatures would yield electrodes of greater porosity and better operational characteristics.

However, the important part of the tests is that which determines the behavior of the electrode operating at a constant load over a period of time (figures 11A,B,C and 12 A,B,C). These results indicate that better electrode properties as determined by the decrease in voltage with time occur when the electrodes have been compacted at pressures of 25,000 or 35,000 psi and sintered at temperatures of 750 or 775° C.

It was noted in the results given above, that one electrode appeared to be much better than the others: DM2-2. This electrode was compacted at a pressure of approximately 25,000 psi for two minutes and then due to an operational difficulty, the pressure increased to 28,700 psi for a few seconds before being released. The electrode was then sintered at 775° C according to the procedure previously noted. The superior results may be explained by the fact that instead of a single-layer double-skeleton electrode having pores of a constant size, the electrode was a double-layer double-skeleton electrode with the surfaces having smaller pores than the interior of the electrode. This is the result of the application of the high pressure for a short time which may affect only the surface. According to Justi[17] and Bacon[7], this type of electrode is superior to single-layer electrodes because it minimizes the

FIGURE IIA - DECAY OF ELECTRODE PROPERTIES WITH TIME AT LOAD FOR ELECTRODES COMPACTED AT 15000 PSI AND SINTERED AT VARIOUS TEMPERATURES

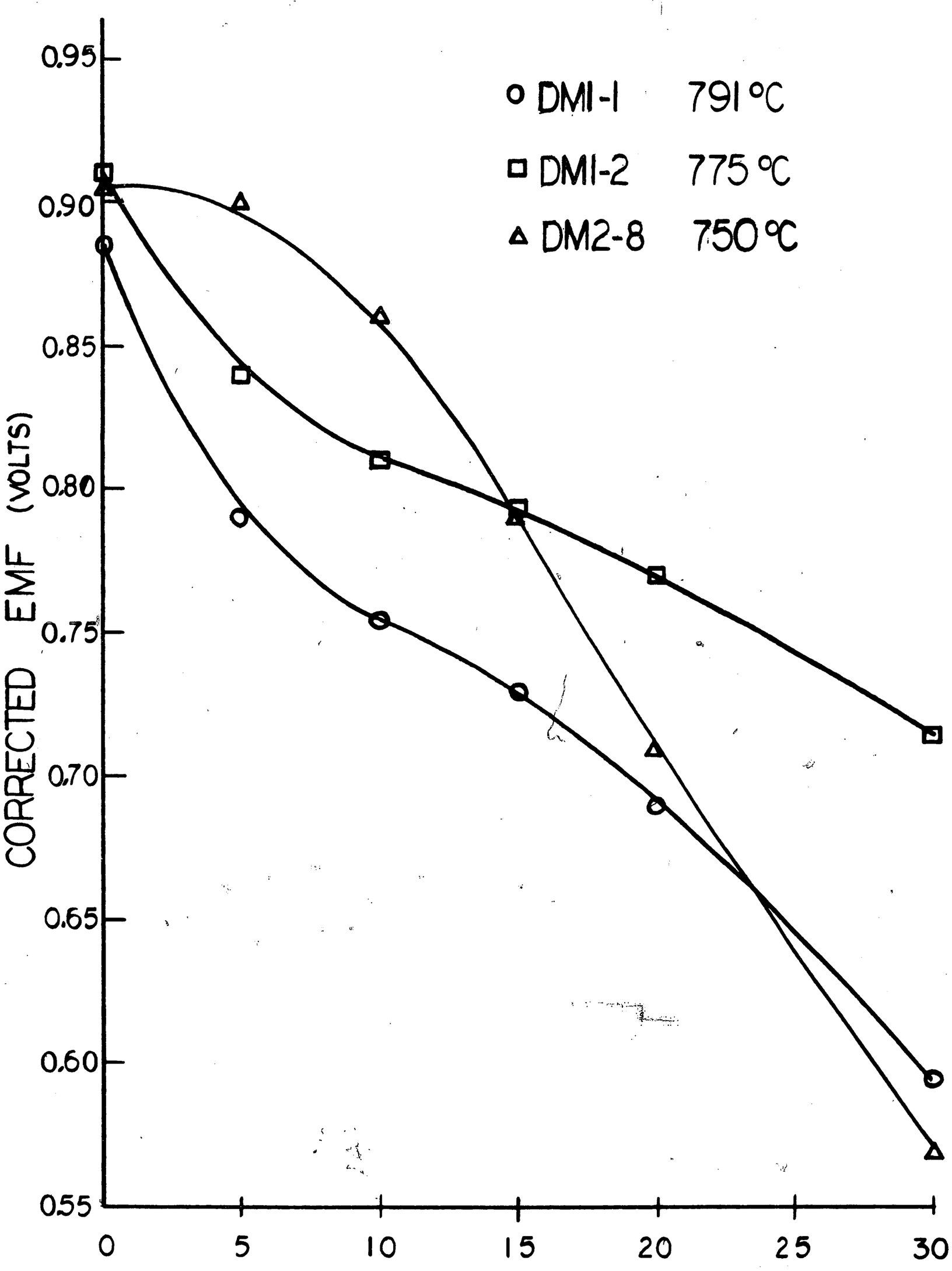

FIGURE 11B - DECAY OF ELECTRODE PROPERTIES WITH TIME AT LOAD FOR ELECTRODES COMPACTED AT 25000 PSI AND SINTERED AT VARIOUS TEMPERATURES

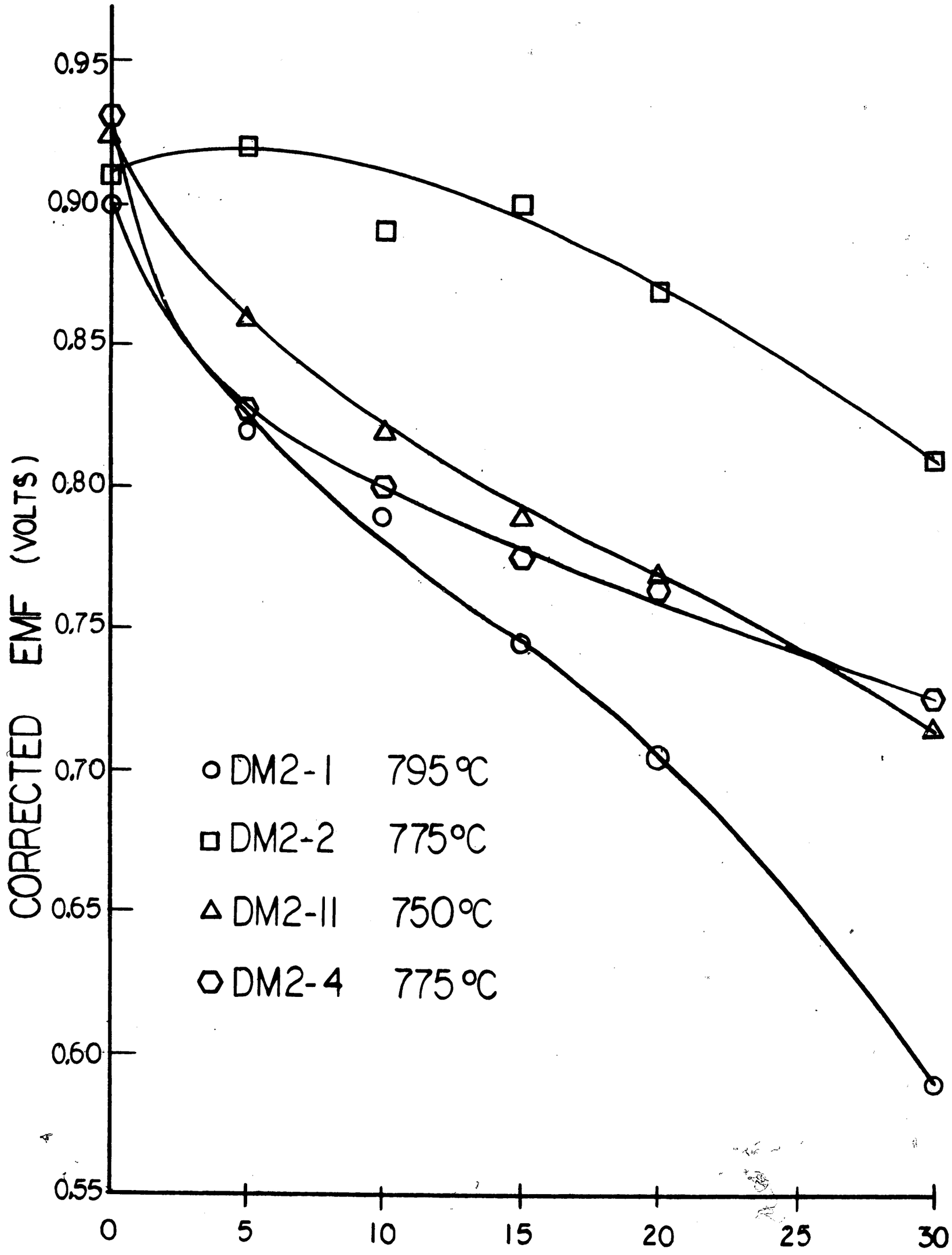

FIGURE 11C - DECAY OF ELECTRODE PROPERTIES WITH TIME AT LOAD FOR ELECTRODES COMPACTED AT 35000 PSI AND SINTERED AT VARIOUS TEMPERATURE

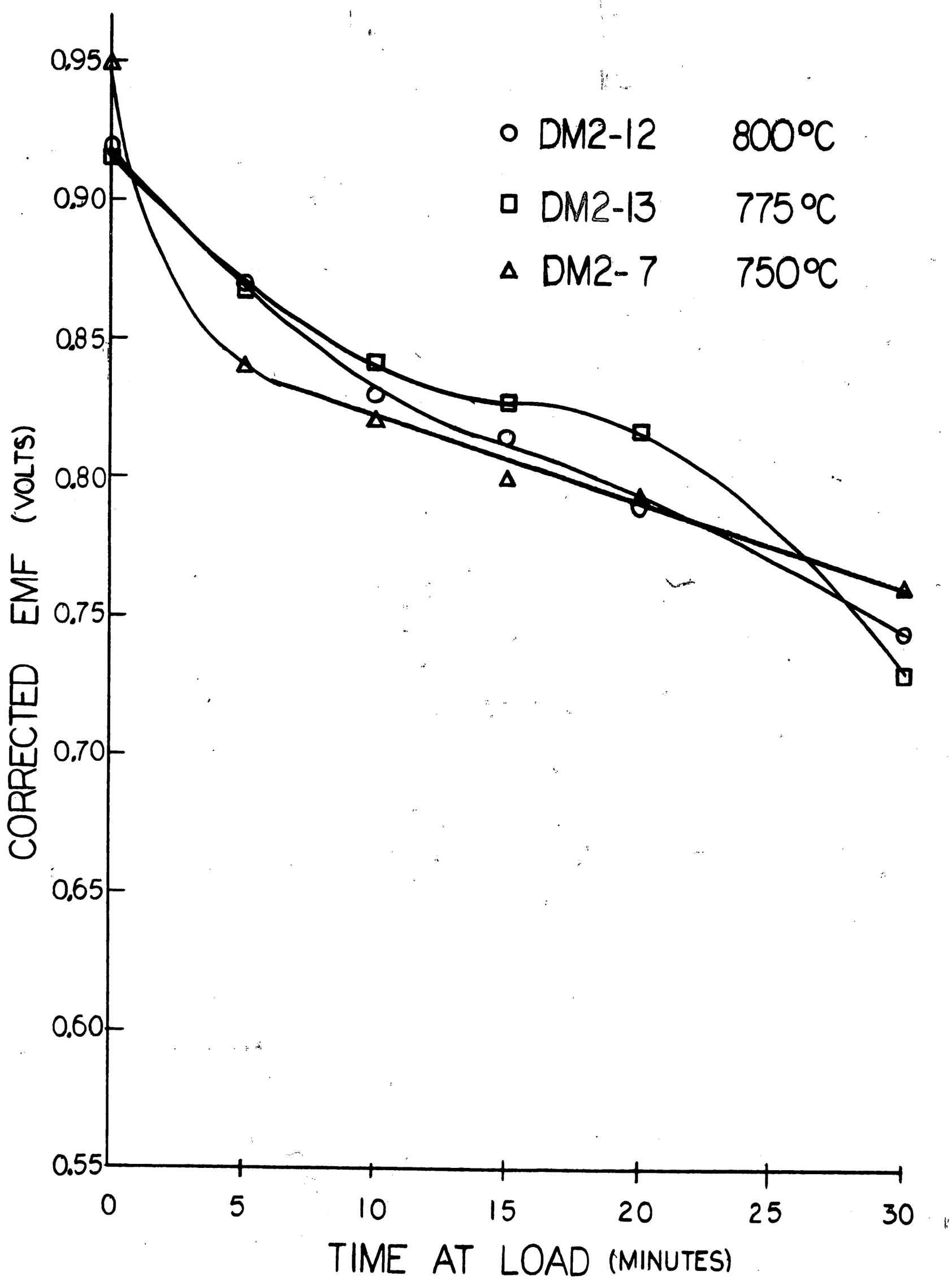

FIGURE 12A-DECAY OF ELECTRODE PROPERTIES WITH TIME AT LOAD FOR ELECTRODES SINTERED AT 750°C AFTER COMPACTING AT VARIOUS PRESSURES

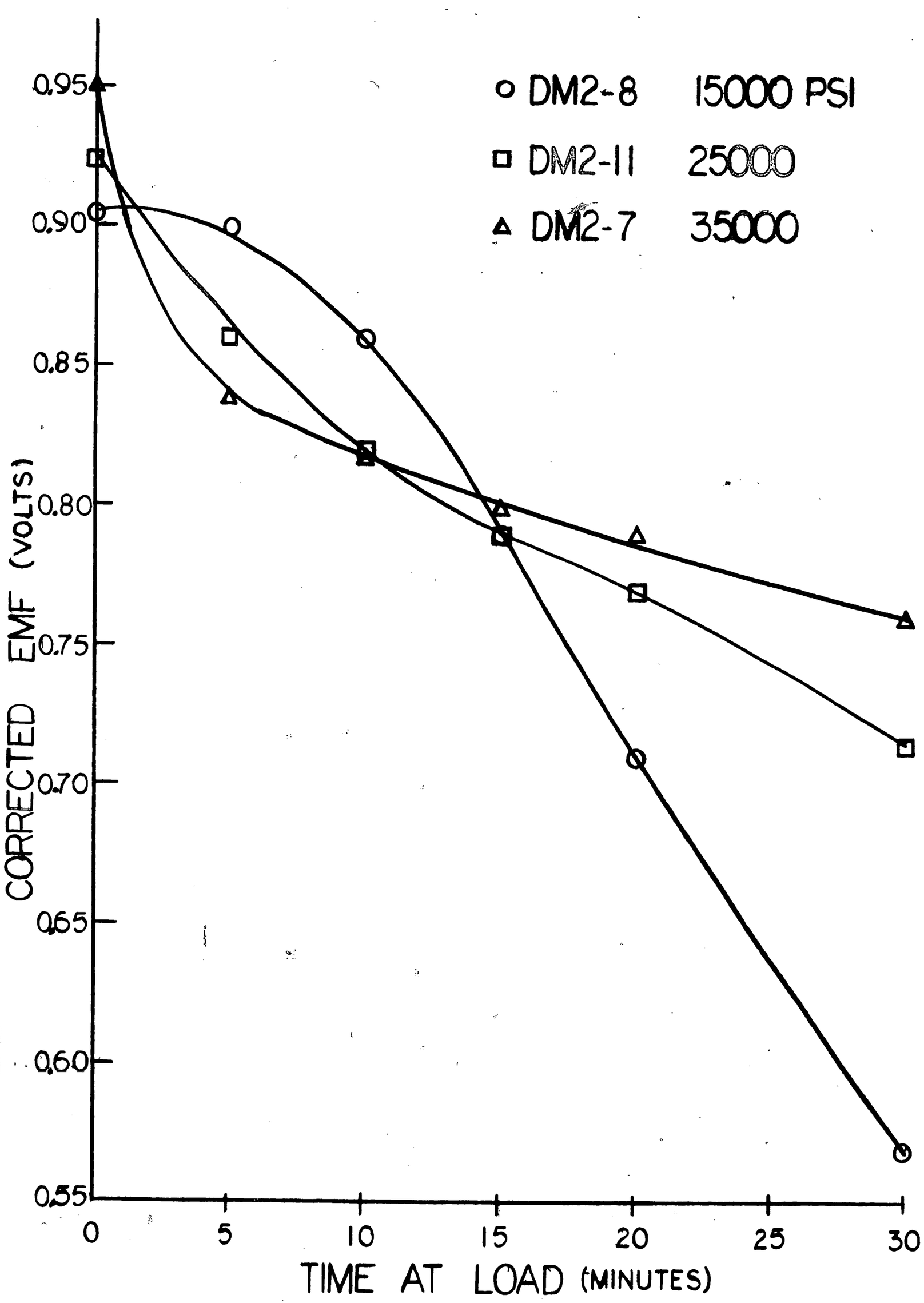

FIGURE 12B - DECAY OF ELECTRODE PROPERTIES WITH TIME AT LOAD FOR ELECTRODES SINTERED AT 775°C AFTER COMPACTING AT VARIOUS PRESSURES

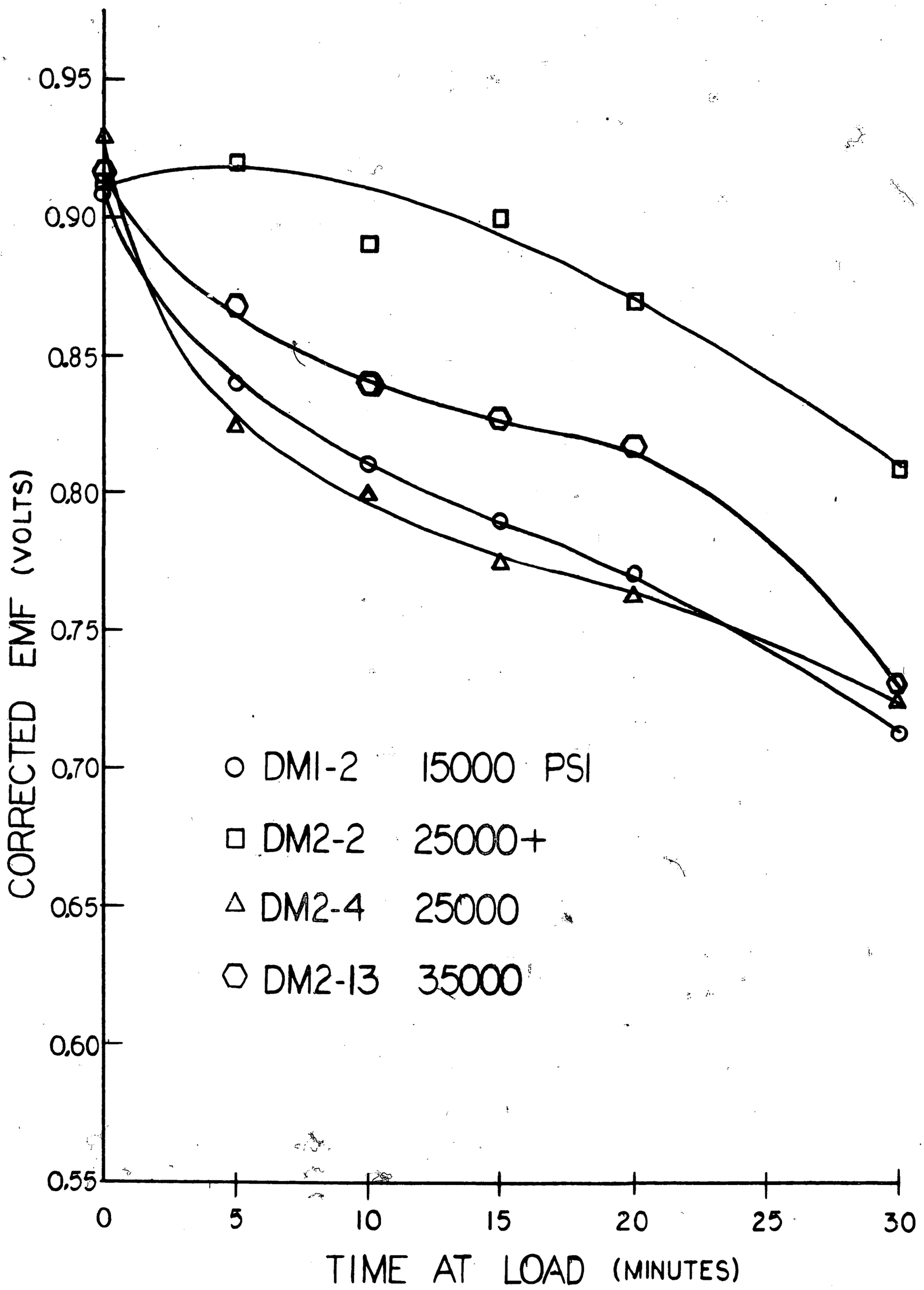

FIGURE 12C - DECAY OF ELECTRODE PROPERTIES WITH TIME AT LOAD FOR ELECTRODES SINTERED AT 795°C AFTER COMPACTING AT VARIOUS PRESSURES

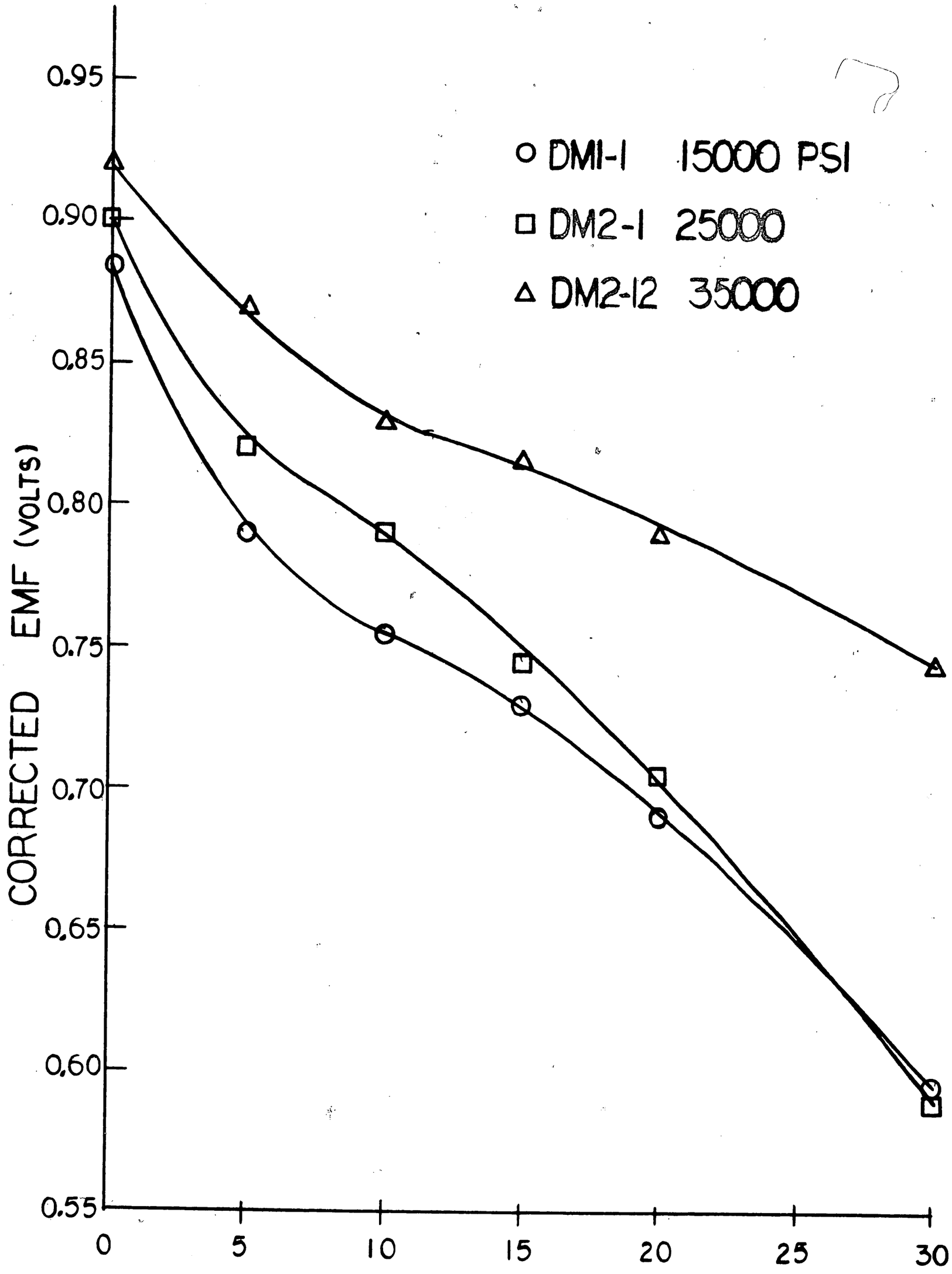

amounts of fuel and electrolyte which migrate completely through the electrode, and thus minimize any "flooding" of the electrode.

As a further test, electrode DM2-10 was compacted at 28,730 psi and sintered at 775° C in order to check the results of electrode DM2-2. In both the constant time and constant current density tests, the results indicate a better electrode than all except DM2-2 and thus lead one to a better approach to the fabrication of electrodes.

B. RESULTS OF X-RAY DIFFRACTION STUDIES

Powder diffraction patterns of the Raney Alloy No. 2813 show that it is a two phase alloy composed of $NiAl_3$ and Ni_2Al_3. This is in agreement with the data presented in the literature[24][33-35] for a Raney alloy of 50 weight per cent nickel and 50 weight per cent aluminum.

Initial activation of loose Raney powder using 6N potassium hydroxide solvent for the aluminum resulted in a catalyst whose powder pattern showed it to be face-centered-cubic nickel. Aluminum may have been present but in such small quantities that it produced no diffraction pattern. This is in agreement with the work of Kokes and Emmett[18-19] which is presented in Table IV and with that of Lainer and Kagan[36]. That the structure was noted to be face-centered-cubic is attributed to the fact that no attempt was made to control the temperature of activation and at higher temperatures, the catalyst lattice has been reported[33][35] to "collapse" to a face-centered-cubic structure.

Table IV. Lattice Parameters of Activated Raney Catalyst

Component	Structure	Lattice Parameters	
		Literature	Experimental[a]
Nickel	fcc	a=3.5238Å	a=3.5206Å
Activated Nickel[b]			
(1) Initial	fcc	a=3.532Å	
(2) Degassed	fcc	a=3.535Å	
Activated Catalyst No. 2813	fcc		a=3.5337Å

(a) Average of several patterns

(b) Kokes and Emmett, J. Am. Chem. Soc. 81 (1959) 5032

A second batch of loose Raney alloy was activated using 6N potassium hydroxide solvent. The temperature of activation was maintained below 50° C. After activation was completed, a sample was taken for X-ray diffraction analysis and the remainder stored in a weak alkaline solution until required for testing. X-ray data for the activated sample is listed in Table V.

After a short time, samples of this activated catalyst were taken for a deactivation study. It has been reported[17][33] that upon heating, the catalyst deteriorates. Samples were placed in a drying oven and heated in air for thirty minutes at temperatures ranging from 75 to 200° C in order to deactivate the catalyst. After the deactivation treatments, X-ray diffraction patterns were taken to determine the effect of deactivation temperature on the catalyst structure.

Analysis of the powder patterns showed that nickel of face-centered-cubic structure was present in all deactivated samples. It was noted that at deactivation temperatures above 125° C, the nickel began to oxidize. It was also noted that evidence of the presence of small traces of $NiAl_3$ could be detected. This indicates that the activation was not complete as would be expected since the maximum activation temperature was 50° C.

Figure 13 and Table V show the "collapse" of the catalyst structure with deactivation temperature. The nickel lattice parameter of the catalyst increases until it approaches

Table V. Temperature Dependent Deactivation Structural Analysis of Raney Catalyst No. 2813

Catalyst Condition	d_{111} Nickel	a_o(Nickel)	a_o(average)
Activated	2.0260Å	3.509Å	3.509Å
75°C Deactivated	2.0286	3.514	
	2.0260	3.509	3.5115
100°C Deactivated	2.0306	3.517	
	2.0299	3.516	3.5165
125°C Deactivated	2.0286	3.514	
	2.0299	3.516	3.515
150°C Deactivated	2.0358	3.526	
	2.0299	3.516	3.521
175°C Deactivated	2.0378	3.529	
	2.0332	3.522	3.5255
200°C Deactivated	2.0326	3.520	
	2.0326	3.520	3.520

Deactivation time was 30 minutes for all samples.

Iron K_α Radiation used for all diffraction patterns.

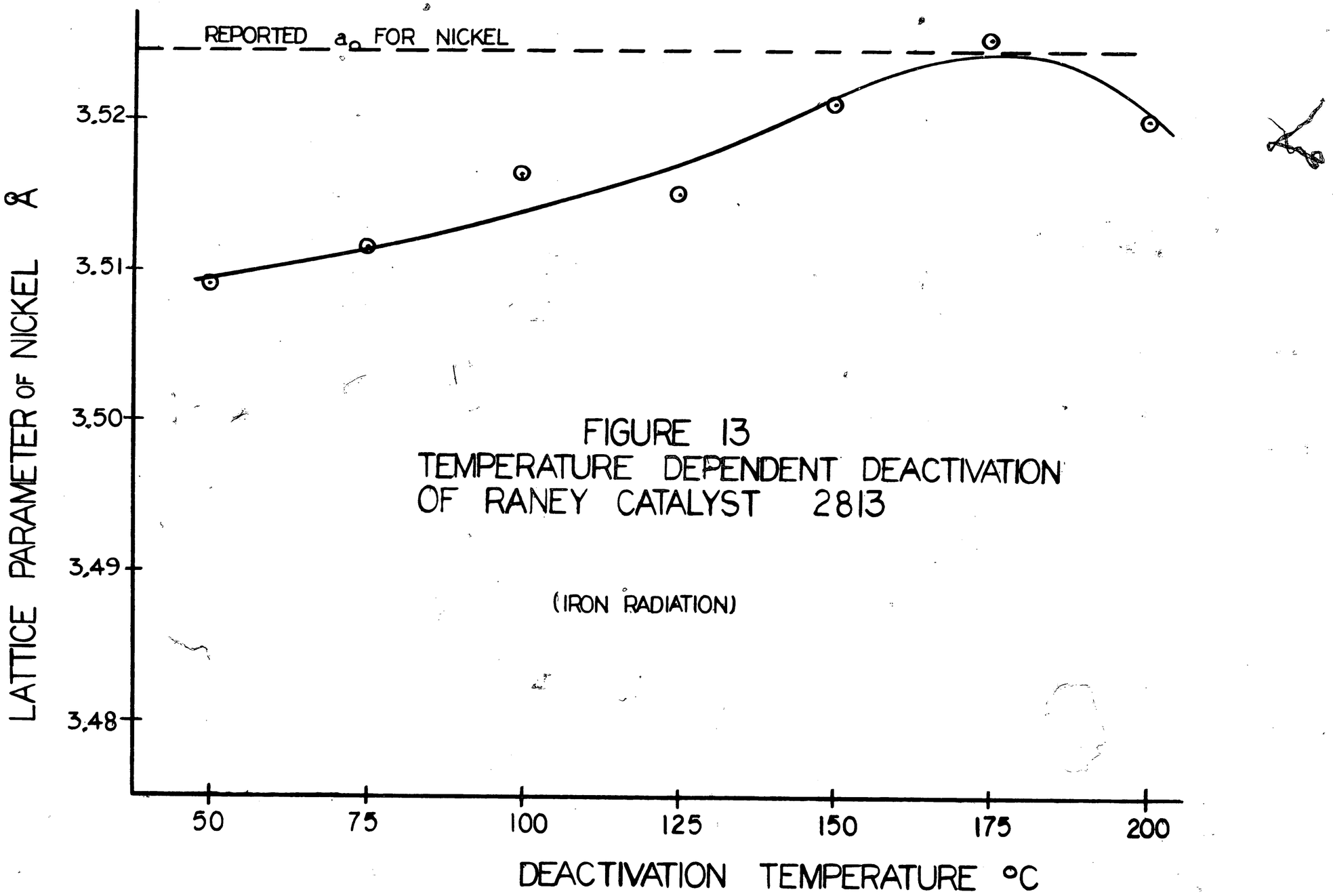

FIGURE 13
TEMPERATURE DEPENDENT DEACTIVATION
OF RANEY CATALYST 2813

(IRON RADIATION)

the lattice parameter of normal pure nickel and then decreases. This "collapsing" of the structure is in agreement with published literature.[18-20][33][35]

A second deactivation test was studied to determine the effect of time at deactivation temperature on the catalyst structure. After activation, a sample of the catalyst was taken for X-ray diffraction structure analysis (results given in Table VI) and deactivation was started immediately. Samples were removed periodically for X-ray diffraction structure analysis.

X-ray diffraction analysis of the samples showed that the activated material and all deactivated samples, except the six-hour deactivation, contained $NiAl_3$ and face-centered-cubic nickel. In general, it appeared that the amount of $NiAl_3$ decreased with increasing time due to the additional leaching effects.

The X-ray data were then analyzed for the variation of lattice parameter of nickel based on the 111 plane spacing as a function of deactivation time (Table VI). A graph of these data (Figure 14) shows that the maximum in lattice parameter occurred after thirty minutes and then a decrease in parameter indicating the lattice "collapse".

After storage in 1N potassium hydroxide solution, X-ray diffraction patterns of the electrodes which showed irregular electrical results (DM2-3, DM2-6, DM2-12, and DM2-13) all showed the material to correspond to face-centered-cubic nickel.

Table VI. Time Dependent Deactivation Structural Analysis of Raney Catalyst No. 2813

Catalyst Condition	d_{111}(Nickel)	a_o(Nickel)	a_o(average)
Activated	2.0254Å	3.508Å	
	2.0314	3.518	3.513Å
15 min. Deactivated	2.0352	3.525	
	2.0372	3,528	3.5265
30 min. Deactivated	2.0339	3.523	
	2.0392	3.532	3.5275
60 min. Deactivated	2.0319	3.519	
	2.0273	3.511	3.515
120 min.Deactivated	2.0306	3.517	
	2.0293	3.515	3.516
240 min.Deactivated(a)			
	2.0234	3.505	
	2.0254	3.508	3.5065
360 min.Deactivated(a)			
	2.0215	3.501	
	2.0209	3.500	3.5005

(a) Results subject to question as container failed and may have contaminated catalyst.

Deactivation temperature is boiling point of 6N KOH solution (110-115° C)

Iron K_α radiation use for all diffraction patterns.

FIGURE 14
TIME DEPENDENT DEACTIVATION
OF RANEY CATALYST 2813

(IRON RADIATION)

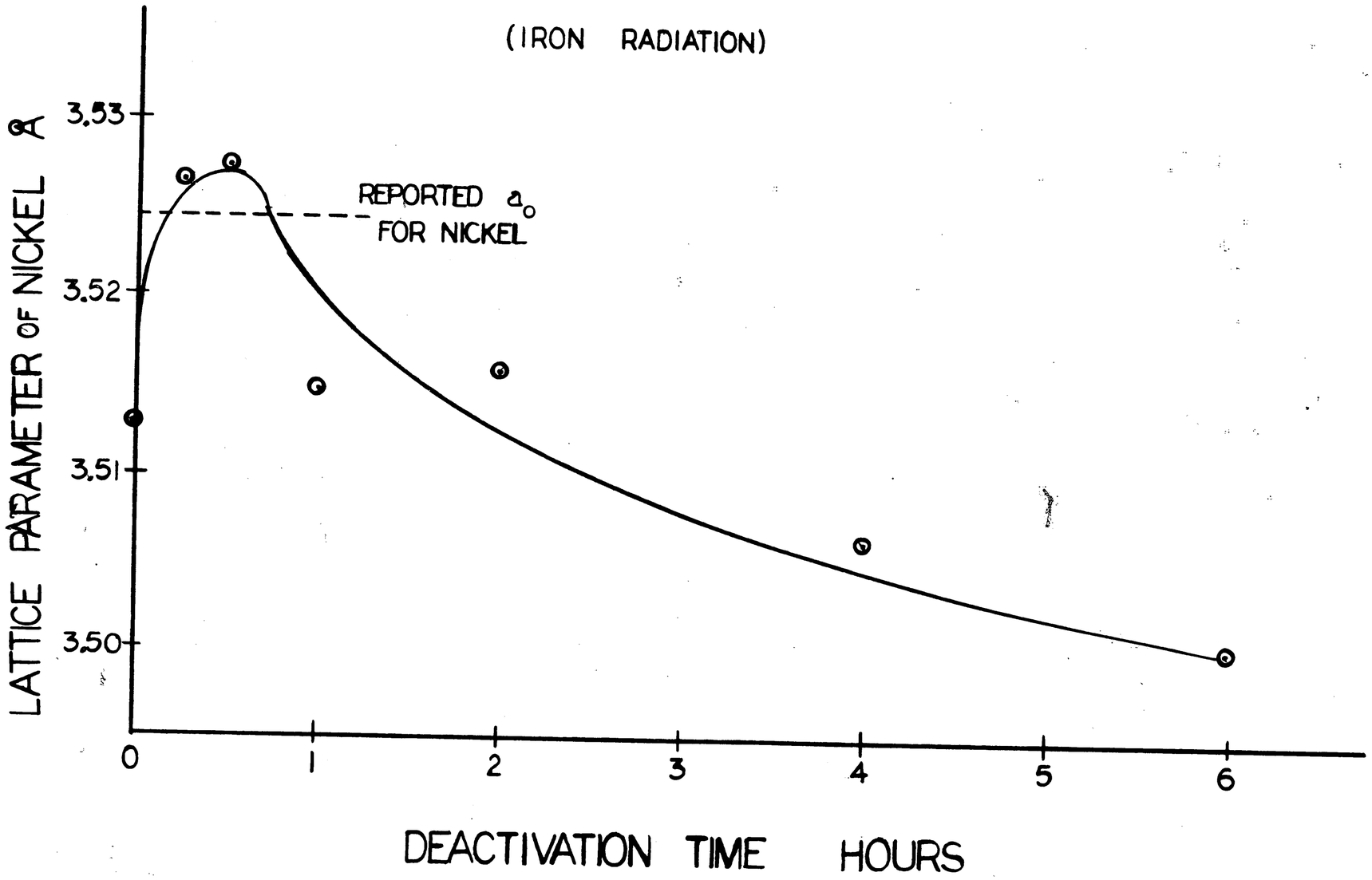

There was no indication of intermediate aluminum-nickel phases being present, thus indicating that activation had apparently been completed. From this, it appears that the irregularities were the properties developed by the various compacting and sintering treatments. However, aluminum may have been present in the form of a solid solution with nickel. This would result in a slight increase in the lattice parameter of nickel but would not produce any extra diffraction lines.

Thus, a further explanation of the irregularities in the electrical properties may be that there were various amounts of aluminum in solution with nickel and this had the same effect as incomplete activation.

CONCLUSIONS AND RECOMMENDATIONS

From the results presented in the previous section, it would appear that a double-layer double-skeleton-catalyst electrode will perform more satisfactorily under the test conditions described than will a single-layer double-skeleton-catalyst electrode. This is shown in the data of electrode DM2-2 and agrees with the literature[7][17]. Also, from the powder metallurgical variables studied, an electrode compacted at a pressure of 28,700 psi and sintered at 775° C will be seen to have maximum operating characteristics for the singularly-pressed electrodes and is second only to the double-pressed material. However, this does not mean that such an electrode will have the maximum possible operating characteristics.

It is recommended that future work should expand the study of the powder metallurgical variables involved in the fabrication of electrodes for use in fuel cells to include a more comprehensive study of compacting pressure, including double pressing, and sintering temperatures. In addition, such work should also include a study of the effect of sintering time and atmosphere, composition of the Raney alloy and the supporting skeleton, and the grain sizes of the Raney alloy and the supporting skeleton, on the operating characteristics of the fuel electrodes.

BIBLIOGRAPHY

1. Liebhafsky, H.A. "Fuel Cells" International Science and Technology. January 1962, p. 54.

2. Douglas, D.L. "Fuel Cells" Elect. Eng. 78, (1959), p. 906.

3. Austin, L.G. "Fuel Cells" Scientific American 201 - No. 4 (October 1959), p. 72.

4. Egli, P.H. "Direct Energy Conversion" Jour. of Metals, August 1960, p. 615.

5. Graduate Students at Harvard Business School. "Fuel Cells - Power for the Future" Fuel Cell Research Associates. Cambridge 38, Mass., Oct. 1960.

6. Young, G. J. "Fuel Cells" Reinhold Publishing Corporation, New York 1960.

7. Bacon, F.T. "Research into the Properties of the Hydrogen-Oxygen Fuel Cell" Beama J. 61 (1954) p. 6.

8. Gorin, E., and Recht, H.L. "Fuel Cells" Chem. Eng. Progress 55 - No. 8 (1959), p. 51.

9. (a) Grove, W. Phil. Mag. 14 (1839), p. 129
   (b) Grove, W. Phil. Mag. 21 (1842), p. 417
   (c) Grove, W. Proc. Roy. Soc. 4 (1843), p. 463
   (d) Grove, W. Proc. Roy. Soc. 5 (1845), p. 557

10. Mond, L. and Langer, C. "A New Form of Gas Battery" Proc. Roy. Soc. 46A (1889), p. 296

11. "12th Annual Battery Research and Development Conference" U. S. Army Signal Research and Development Laboratory. April 1959, p. 105-124.

12. "13th Annual Power Sources Research Conference" U. S. Army Signal Research and Development Laboratory. April 1959, p. 105-124.

13. "14th Annual Power Sources Research Conference" U. S. Army Signal Research and Development Laboratory. May 1960, p. 50-77.

14. Stein, B.R. "Status Report on Fuel Cells" ARO Report No. 1 June 1959. PB 151804, U. S. Dept. of Commerce - O.T.S.

15. Stein, B.R., and Cohn, E.M. "Second Status Report on Fuel Cells" ARO Report No. 2, Dec. 1960. PB171155 U.S.Department of Commerce - O.T.S.

16. De Zubay, E.A., and Shultz, E.B. "Fuel Cells" Industrial Research 3 - No. 4 (Oct. 1961), p. 19.

17. Justi, E., Pilkuhn, M., Scheibe, W., and Winsel, A. "High-Drain Hydrogen-Diffusion-Electrode Operating at Ambient Temperature and Low Pressure" 1959. Translated by Burton, Research Information Service, Division Pergamon International Corporation.

18. Kokes, R.J., and Emmett, P.H. "The Role of Hydrogen in Raney Nickel Catalysts" Jour. Amer. Chem. Soc. 81 (1959), p. 5032.

19. Kokes, R.J., and Emmett, P.H. "The Activity of Raney Nickel as a Function of Hydrogen Content" Jour. Amer. Chem. Soc. 82 (1960), p. 4497.

20. Lieber, E., and Morritz, F.L. "The Uses of Raney Nickel" Advances in Catalysis Vol. V., Academic Press Inc., New York, 1953, p. 417.

21. Raney, M. "Catalysts from Alloys - Nickel Catalysts" Ind. and Eng. Chem. 32 (1940), p. 1199.

22. Raney, M. U. S. Patent 1,563,587 (Dec. 1, 1925)

23. Raney, M. U. S. Patent 1,628,190 (May 10, 1927)

24. Hansen, M. "Constitution of Binary Alloys" McGraw-Hill Book Co., Inc., New York, 1958, p. 118

25. Adkins, H., and Billica, H.R. "The Preparation of Raney Nickel Catalysts and Their Use Under Conditions Comparable with Those for Platinum and Palladium Catalysts" Jour. Amer. Chem. Soc. 70 (1948), p. 695.

26. Smith, H.A., Bedoit, W.C., and Fuzek, J.F. "The Preparation and Aging of Raney Nickel Catalysts" Jour. Amer. Chem. Soc. 71 (1949), p. 3769.

27. Ipatieff, V.M., and Pines, H. "Composition of W-6 Raney Nickel Catalysts" Jour. Amer. Chem. Soc. 72 (1950), p. 5320.

28. Pavlic, A.A., and Adkins, H. "Preparation of Raney Nickel Catalyst" Jour. Amer. Chem. Soc. 68 (1946) p. 1471

29. Mozingo, R. Org. Synthesis 21 (1941), p. 15.

30. Bond, G.C. "Catalysis by Metals" Academic Press, New York, 1962, p. 34-35.

31. Covert, L.W., and Adkins, H. Jour. Amer. Chem. Soc. 54 (1932), p. 4116.

32. Sun Oil Company "Standard Test Procedures for Fuel Cell Electrodes" Nov. 21, 1961 (unpublished)

33. Littman, H.L., and Dew-Hughes, B. "Catalyst Structures and Properties" Ind. and Eng. Chem. 51 (1959) p. 662

34. (a) Bradley, A.J., and Taylor, A. "An X-ray Analysis of the Ni-Al System" Proc. Roy. Soc. (London) 159A (1937), p. 56

(b) Bradley, A.J., and Taylor, A. Phil. Mag. 23 (1937) p. 1049.

35. Taylor, A., and Weiss, J. "Defect Lattices and Catalytic Activity" Nature 141 (1938), p. 1055.

36. Lainer, D.I., and Kagan, N.M. "The Phase Composition of Catalysts Produced by Leaching Al-Ni Alloys" The Physics of Metals and Metallography 11 - No. 6, (1961), p. 16.

VITA

John R. Thompson, Jr., the son of John R. and Jane W. Thompson, was born in Kane, Pennsylvania, on August 10, 1937. He received his primary and secondary education in the Kane Public School System, graduating from Kane Area Joint High School in June 1955. In September of 1955 he enrolled at the University of Cincinnati where he had been awarded a Dresser Manufacturing Division Scholarship. The degree of Bachelor of Science in Metallurgical Engineering was conferred upon him in June 1960. During his undergraduate education, John did his co-operative work with the Dresser Manufacturing Division of Bradford, Pennsylvania.

During the summer of 1960, John was employed as a technician in the Research Department of the Bethlehem Steel Corporation located in Bethlehem, Pennsylvania.

In September of 1960, the author enrolled in the Graduate School at Lehigh University in Bethlehem, Pennsylvania. Since that time he has been employed as a research assistant and an instructor in the Department of Metallurgy, Lehigh University.

Professional affiliations are with the American Society for Metals and the American Society for Testing and Materials. The author is a member of Tau Beta Pi, national engineering honorary society, and Alpha Sigma Mu, honorary society for metallurgical engineers.